Cell Reports

Article

YTHDF1-CLOCK axis contributes to pathogenesis of allergic airway inflammation through LLPS

Graphical abstract

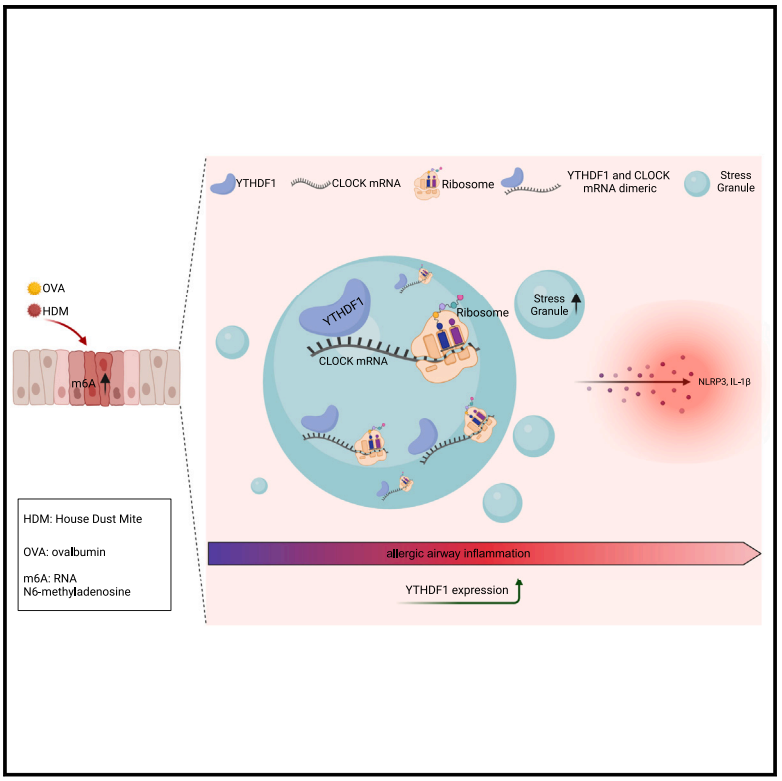

Highlights

- YTHDF1 modulates proinflammatory responses in allergic airway epithelial cells
- YTHDF1 augments CLOCK translation in an m6A-dependent manner
- Allergens enhance YTHDF1 liquid-liquid phase separation to form a complex with CLOCK mRNA
- YTHDF1 regulates NLRP3 inflammasome generation and IL-1β secretion through CLOCK

Authors

Jing Wang, Yao Zhou, Meng Zhang, ..., Jiajia Lv, Min Wu, Zhenwei Xia

Correspondence

xzw10484@rjh.com.cn (Z.X.), 19880316@163.com (J.L.), minwoo2022@126.com (M.W.), tina_tangwei@163.com (W.T.)

In brief

Wang et al. evaluate the impact of YTHDF1 on allergic airway inflammation, explore the mechanism by which YTHDF1 regulates the target gene CLOCK by forming a complex with CLOCK mRNA through liquid-liquid phase separation and migration into stress granules, and further infer its clinical relevance in human subjects.

Wang et al., 2024, Cell Reports *43*, 113947
March 26, 2024
https://doi.org/10.1016/j.celrep.2024.113947

CellPress

Cell Reports

CellPress
OPEN ACCESS

Article

YTHDF1-CLOCK axis contributes to pathogenesis of allergic airway inflammation through LLPS

Jing Wang,[1,2,6] Yao Zhou,[1,6] Meng Zhang,[1,6] Yujiao Wu,[1] Qun Wu,[1] Wen Su,[1] Min Xu,[2] Jinhong Wu,[2] Min Zhang,[2] Jianwei Shuai,[4,5] Wei Tang,[3,*] Jiajia Lv,[1,*] Min Wu,[4,5,7,*] and Zhenwei Xia[1,7,8,*]

[1]Department of Pediatrics, Ruijin Hospital, Shanghai Jiao Tong University School of Medicine, Shanghai, China
[2]Department of Surgery, Shanghai Children's Medical Center, Shanghai Jiao Tong University School of Medicine, Shanghai, China
[3]Department of Pulmonary and Critical Care Medicine, Ruijin Hospital, Shanghai Jiao Tong University School of Medicine, Shanghai, China
[4]Joint Research Centre on Medicine, The Affiliated Xiangshan Hospital of Wenzhou Medical University, Ningbo, China
[5]Wenzhou Institute, University of Chinese Academy of Sciences, Wenzhou, China
[6]These authors contributed equally
[7]Senior author
[8]Lead contact
*Correspondence: tina_tangwei@163.com (W.T.), 19880316@163.com (J.L.), minwoo2022@126.com (M.W.), xzw10484@rjh.com.cn (Z.X.)
https://doi.org/10.1016/j.celrep.2024.113947

SUMMARY

N6-methyladenosine (m6A) modification has been implicated in many cell processes and diseases. YTHDF1, a translation-facilitating m6A reader, has not been previously shown to be related to allergic airway inflammation. Here, we report that YTHDF1 is highly expressed in allergic airway epithelial cells and asthmatic patients and that it influences proinflammatory responses. CLOCK, a subunit of the circadian clock pathway, is the direct target of YTHDF1. YTHDF1 augments CLOCK translation in an m6A-dependent manner. Allergens enhance the liquid-liquid phase separation (LLPS) of YTHDF1 and drive the formation of a complex comprising dimeric YTHDF1 and CLOCK mRNA, which is distributed to stress granules. Moreover, YTHDF1 strongly activates NLRP3 inflammasome production and interleukin-1β secretion leading to airway inflammatory responses, but these phenotypes are abolished by deleting CLOCK. These findings demonstrate that YTHDF1 is an important regulator of asthmatic airway inflammation, suggesting a potential therapeutic target for allergic airway inflammation.

INTRODUCTION

Asthma is an allergic disease that affects approximately 300 million people worldwide and causes approximately 250,000 deaths annually.[1] Among the most important scientific advances in recent years, epigenetic modifications play critical roles in mediating the interaction between genes and the environment, robustly influencing the course of many diseases.[2–5] The in-depth study of the epigenetic mechanisms for asthma development may facilitate the discovery of biomarkers and effective treatment strategies for asthmatic conditions.[6,7]

Epigenetics typically refers to DNA methylation, histone modification, and RNA modification.[8–10] RNA N6-methyladenosine (m6A) is considered the most prevalent, abundant, and conserved internal transcriptional modification of eukaryotic mRNAs.[11–14] m6A modification mediates the recruitment of m6A readers that associate m6A-modified RNAs with mRNA-processing enzymes to influence RNA export, splicing, translation, and degradation.[15–18] YTHDF1 has been identified as a translation-facilitating m6A reader that recruits translation machinery to its target mRNAs in the cytoplasm.[19,20] Recent studies have revealed that YTHDF1 plays crucial roles in various physiological processes, such as cell proliferation and epithelial-mesenchymal transition of cancer cells.[21,22] However, the clinical significance and molecular mechanisms for the effects of YTHDF1 in asthma have not been investigated to date.

Liquid-liquid phase separation (LLPS) is linked to the dynamic formation of membraneless compartments, including stress granules (SGs), P bodies, and nucleoli.[23–25] YTHDF1–3 have been implicated in SG proteome development and interact with SG components.[26–28] Studies revealed that YTHDF1–3 undergo LLPS *in vitro* and in cells and that LLPS is markedly enhanced by mRNAs that contain multiple, rather than single, m6A residues.[29,30] m6A-mRNA interaction is subjected to compartment-specific regulation, including regulated mRNA stability and translation.[31–33] However, there is limited research on the mechanism of YTHDF1 LLPS in allergic airway inflammation.

To narrow the above knowledge gaps, we assessed the impact of YTHDF1 on allergic airway inflammation, explored the mechanism by which YTHDF1 regulated the target gene CLOCK, and further inferred the clinical significance of its action in human subjects.

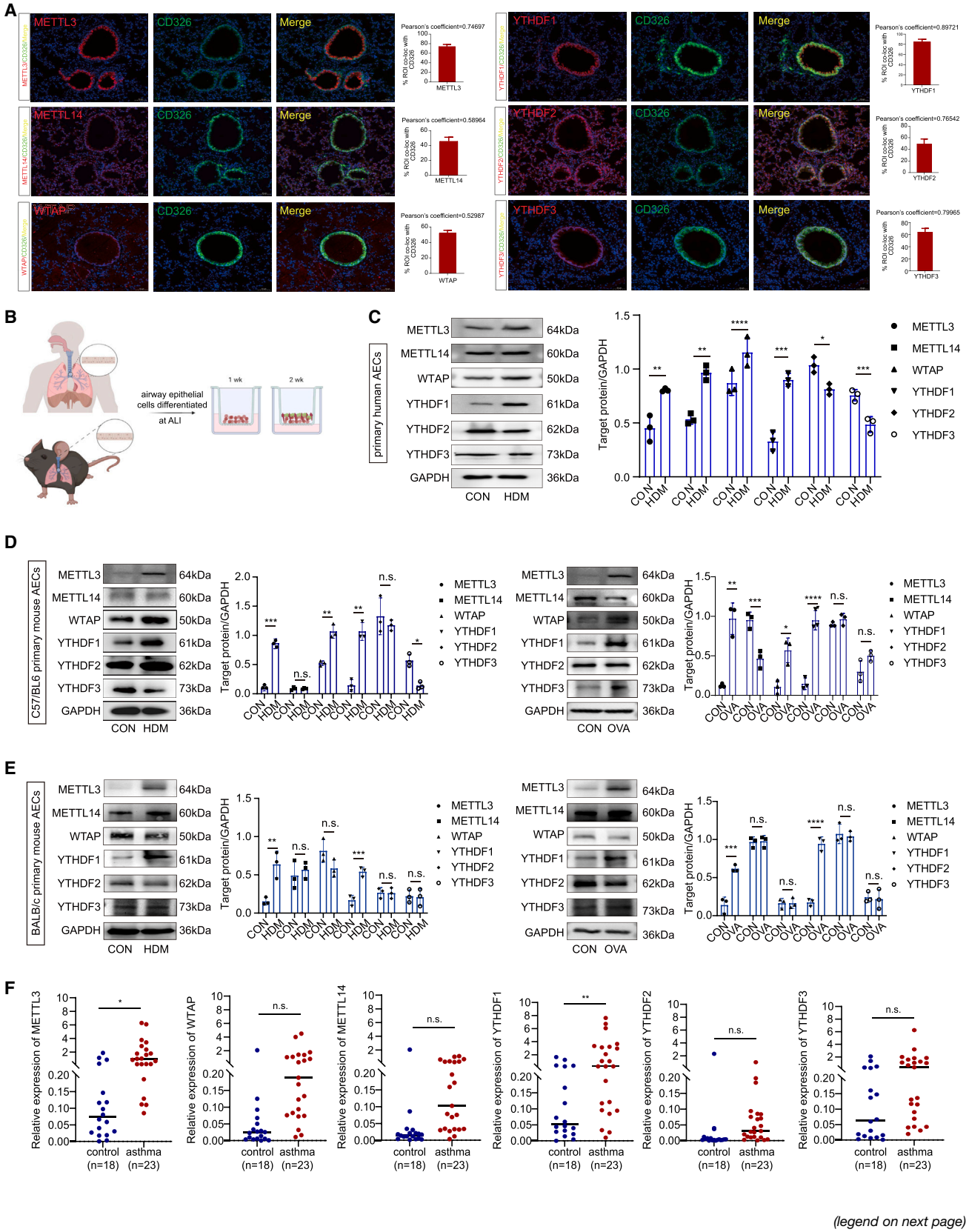

(legend on next page)

RESULTS

m6A is highly regulated in AECs of allergic airway inflammation and YTHDF1 may be a potential biomarker for patients with asthma

In order to detect the expression of m6A regulators in allergic mouse airway epithelial cells (AECs), we applied a classical house dust mite (HDM) allergic airway inflammation mouse model (Figure S1A) and detected a series of inflammation related indicators. Our data indicate the successful establishment of allergic mouse models (Figures S1B–S1F). Using immunofluorescence to evaluate the location of m6A regulators, we found that METTL3 and YTHDF1 were primarily expressed in AECs with the HDM model and control mice (Figures 1A and S1G). The primary human and mouse AECs from control subjects were cultured in the air-liquid interface (ALI) environment (Figure 1B). The newly obtained primary cells were cultured in PneumaCult-Ex Plus medium, and the purity of human and mouse basal cells were about 95% and 98%, respectively (Figures S2A and S2C). After cells filled the entire pore chamber, PneumaCult-ALI medium was used to culture the primary cells for differentiation (Figures S2B and S2D). We evaluated the expression of m6A regulators in HDM-treated primary human AECs and BEAS-2B cells by immunoblotting and RT-qPCR assay and found that METTL3 and YTHDF1 were upregulated in the HDM group (Figures 1C and S2E–S2G). To determine whether these findings depend on mouse strain background and allergen type, we used primary mouse AECs from the C57/BL6 or BALB/c strain and the HDM or ovalbumin (OVA) allergen. In the C57/BL6 or BALB/c strain primary mouse AECs, HDM- or OVA-induced allergic airway inflammation led to an increase in METTL3 and YTHDF1 expression consistently (Figures 1D, 1E, S2H, and S2I). These results indicate that our findings were not strain or allergen dependent. In addition, we used endotoxin-free OVA (EF-OVA), to exclude the effect of OVA-contaminated endotoxin, to stimulate BEAS-2B. We found that both general-OVA and EF-OVA increased YTHDF1 expression and inflammatory responses without significant difference between the two groups, indicating that OVA, but not contaminated endotoxin, is attributed to the induction of YTHDF1 expression and subsequent inflammatory response (Figure S2J). Since METTL3 and YTHDF1 play important roles in m6A modification, we speculate that AECs may be more broadly associated with altered expression of factors that regulate m6A methylation.

Downstream effects of m6A on mRNA translation, export, and stability are mostly determined by the specific readers that recognize modified targets.[34] Therefore, we measured the levels of YTHDF1–3, the main readers in m6A modification, and found that YTHDF1 was primarily enriched and upregulated in allergic AECs. More than that, we sought to determine whether the levels of YTHDF1 in bronchofiberscope brush biopsy specimens obtained from patients with asthma would be the same as those in our model experiments. We validated m6A-related gene mRNA levels in bronchofiberscope brush biopsy specimens obtained from 18 control subjects and 23 patients with asthma. YTHDF1 and METTL3 expression levels were significantly higher in patients with asthma than in control subjects (Figure 1F). In addition, YTHDF1 and METTL3 protein levels were higher in the patients with asthma than in the control subjects (Figure S3A). Among them, the upregulation of YTHDF1 protein is the most significant one. Immunohistochemistry (IHC) demonstrated positive YTHDF1 staining in AECs and higher YTHDF1 expression in the patients with asthma (Figure S3B). In addition, YTHDF1 expression negatively correlated with FEV_1/FVC (forced expiratory volume in 1 second and the forced vital capacity), and similar correlations were observed for percentage changes with predicted FEV_1 (Figure S3C). The ROC (receiver operating characteristic) curves of YTHDF1 expression levels showed the difference between patients with asthma and control subjects (Figure S3D). Collectively, these data provide strong evidence that YTHDF1 may play a crucial role in the pathogenesis of asthma and may be a potential biomarker, as well as a potential drug target, to reduce the suffering of patients with asthma in the clinic.

YTHDF1 induces allergic airway inflammation in AECs

To determine whether YTHDF1 is functionally important in allergic airway inflammation, we knocked down the YTHDF1 gene in primary human AECs and BEAS-2B cells, which led to marked decreases in NLRP3, interleukin-1β (IL-1β), TSLP (thymic dtromal lymphopoietin), IL-25, and IL-33 expression (Figures 2A, 2B, S4A, and S4B). Similar results were obtained with knocking down YTHDF1 in primary AECs from C57/BL6 or BALB/c mice that were treated with HDM or OVA (Figures 2C, 2D, and S4C–S4E). In contrast, overexpression of the YTHDF1 gene reversed the inflammatory response (Figures 2E–2H and

Figure 1. m6A is highly regulated in allergic human and mouse AECs

(A) Immunofluorescence (IF) staining of HDM model of C57/BL6 mouse lung biopsy for METTL3, METTL14, WTAP, YTHDF1, YTHDF2, and YTHDF3 in allergic mice. Scale bars: 50 μm. The bar graph shows the percentage of the region of interest (ROI) colocalized with CD326. Pearson's correlation analyses were used to analyze correlations (n = 4 mice per group).

(B) Primary AEC ALI cultures obtained from bronchofiberscope brush biopsy specimens of control subjects.

(C) Immunoblots analyzing the levels of METTL3, METTL14, WTAP, YTHDF1, YTHDF2, and YTHDF3 in primary human AECs (n = 3–4 subjects per group). All protein ratios derived from the values against GAPDH in CON (control) and HDM groups were plotted as histograms.

(D) Immunoblots of METTL3, METTL14, WTAP, YTHDF1, YTHDF2, and YTHDF3 in HDM- or OVA-stimulated C57/BL6 primary mouse AECs (n = 3–5 mice per group). All protein ratios derived from the values against GAPDH in control and HDM groups were plotted as histograms.

(E) Immunoblots of METTL3, METTL14, WTAP, YTHDF1, YTHDF2, and YTHDF3 in HDM- or OVA-stimulated BALB/c primary mouse AECs (n = 3–5 mice per group). All protein ratios derived from the values against GAPDH in control and HDM groups were plotted as histograms.

(F) RT-qPCR quantifying the relative levels of METTL3, METTL14, WTAP, YTHDF1, YTHDF2, and YTHDF3 in lung tissues from bronchofiberscopy brush biopsy of patients with asthma or control subjects (n = 18 control subjects, n = 23 asthmatic subjects).

Data are shown as the mean ± SEM and are representative of three independent experiments. *$p < 0.05$, **$p < 0.01$, ***$p < 0.001$, and ****$p < 0.0001$; n.s., no statistical significance. Student's t test in (A) and (C)–(E).

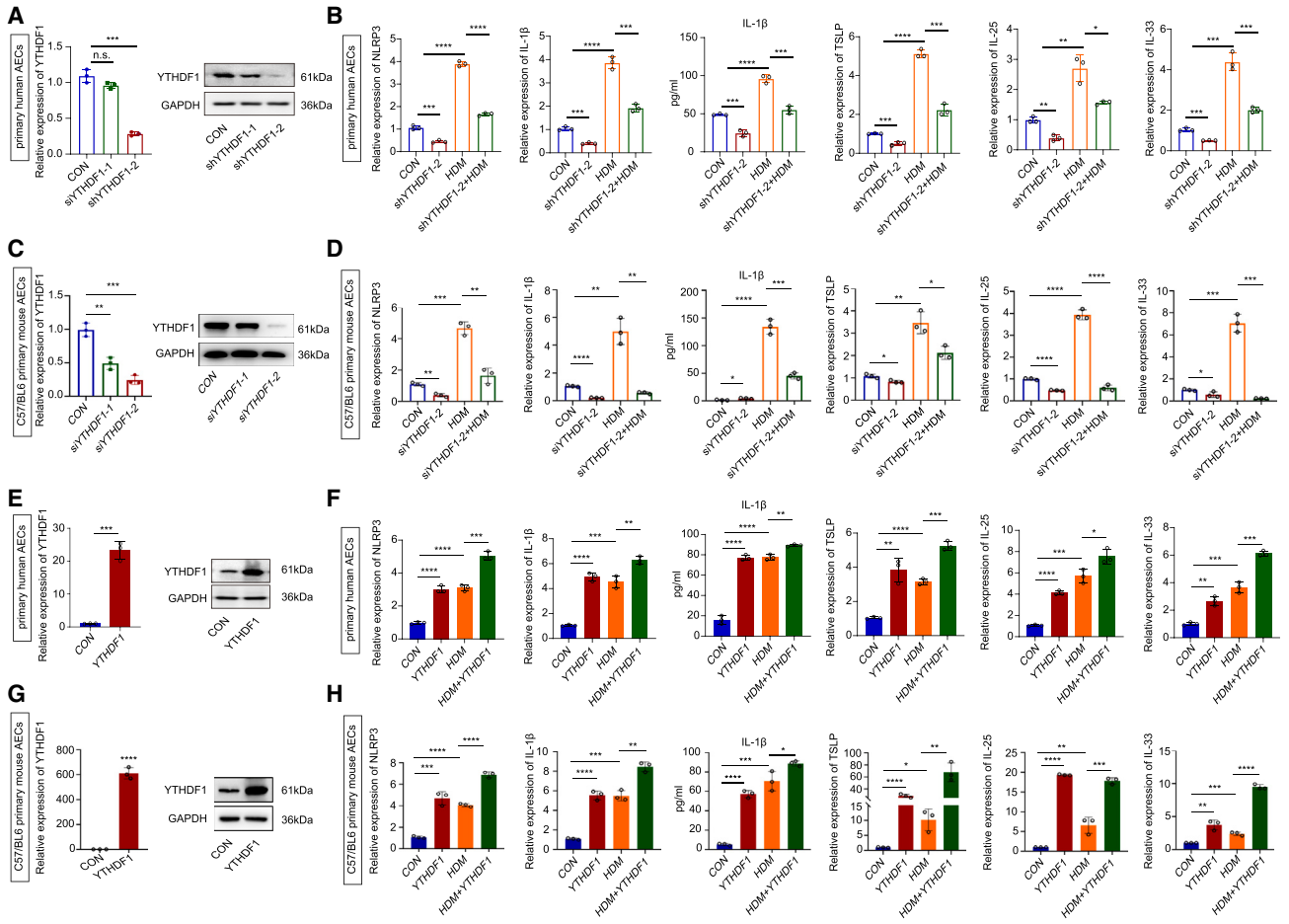

Figure 2. YTHDF1 induces inflammation in AECs stimulated by allergens

(A) RT-qPCR and immunoblots detecting siYTHDF1 (small interfering YTHDF1) effects on primary human AECs (n = 3–4 subjects per group).

(B) RT-qPCR evaluating the expression of NLRP3, IL-1β, TSLP, IL-25, and IL-33 in primary human AECs and ELISA analyzing concentrations of IL-1β in primary human AECs (n = 3–4 subjects per group).

(C) RT-qPCR and immunoblots detecting the siYTHDF1 effects in C57/BL6 primary mouse AECs (n = 3–5 mice per group).

(D) RT-qPCR evaluating the expression of NLRP3, IL-1β, TSLP, IL-25, and IL-33 in C57/BL6 primary mouse AECs and ELISA analyzing the concentrations of IL-1β in primary mouse AEC supernatant (n = 3–5 mice per group).

(E) RT-qPCR and immunoblots detecting YTHDF1 overexpression effects in primary human AECs (n = 3–4 subjects per group).

(F) RT-qPCR evaluating the expression of NLRP3, IL-1β, TSLP, IL-25, and IL-33 in primary human AECs and ELISA analyzing the concentrations of IL-1β in primary human AEC supernatant (n = 3–4 subjects per group).

(G) RT-qPCR and immunoblots detecting YTHDF1 overexpression effects in primary mouse AECs (n = 3–5 mice per group).

(H) RT-qPCR evaluating the expression of NLRP3, IL-1β, TSLP, IL-25, and IL-33 in primary mouse AECs and ELISA analyzing the concentrations of IL-1β in primary mouse AEC supernatant (n = 3–5 mice per group).

Data are shown as the mean ± SEM and are representative of three independent experiments. *p < 0.05, **p < 0.01, ***p < 0.001, and ****p < 0.0001; n.s., no statistical significance. One-way ANOVA with Dunnett's multiple comparison test in (A)–(D), (F), and (H) and Student's t test in (E) and (G).

S4F–S4I). Thus, our results indicate that YTHDF1, as the reader of m6A methylation, promoted an inflammatory response that is strain and allergen independent. To further understand the role of YTHDF1 in allergic airway inflammation, *YTHDF1*$^{fl/fl}$*shh*$^{cre/+}$ mice were challenged with HDM. The IHC data showed that the intensity of the inflammatory response was significantly decreased in the AECs from *YTHDF1*$^{fl/fl}$*shh*$^{cre/+}$ mice (Figure S4J). Periodic acid-Schiff staining results corroborated with the IHC findings: the inflammatory response was decreased in *YTHDF1*$^{fl/fl}$*shh*$^{cre/+}$ mice (Figure S4K). Flexivent data showed down-regulation of airway resistance in *YTHDF1*$^{fl/fl}$*shh*$^{cre/+}$ mice (Figure S4L). Diff-Quik staining and ELISA analysis demonstrate reduced inflammation responses in *YTHDF1*$^{fl/fl}$*shh*$^{cre/+}$ mice compared to the wild-type (WT) counterpart animals (Figure S4M). These data were consistent with the *in vitro* results.

Widespread m6A modification and identification of important biological pathways with altered methylation in allergic mouse AECs

To obtain a transcriptome-wide m6A map in allergic airway inflammation, we performed m6A sequencing (m6A-seq) analysis of AECs from normal and allergic mice *in vivo*. m6A-seq

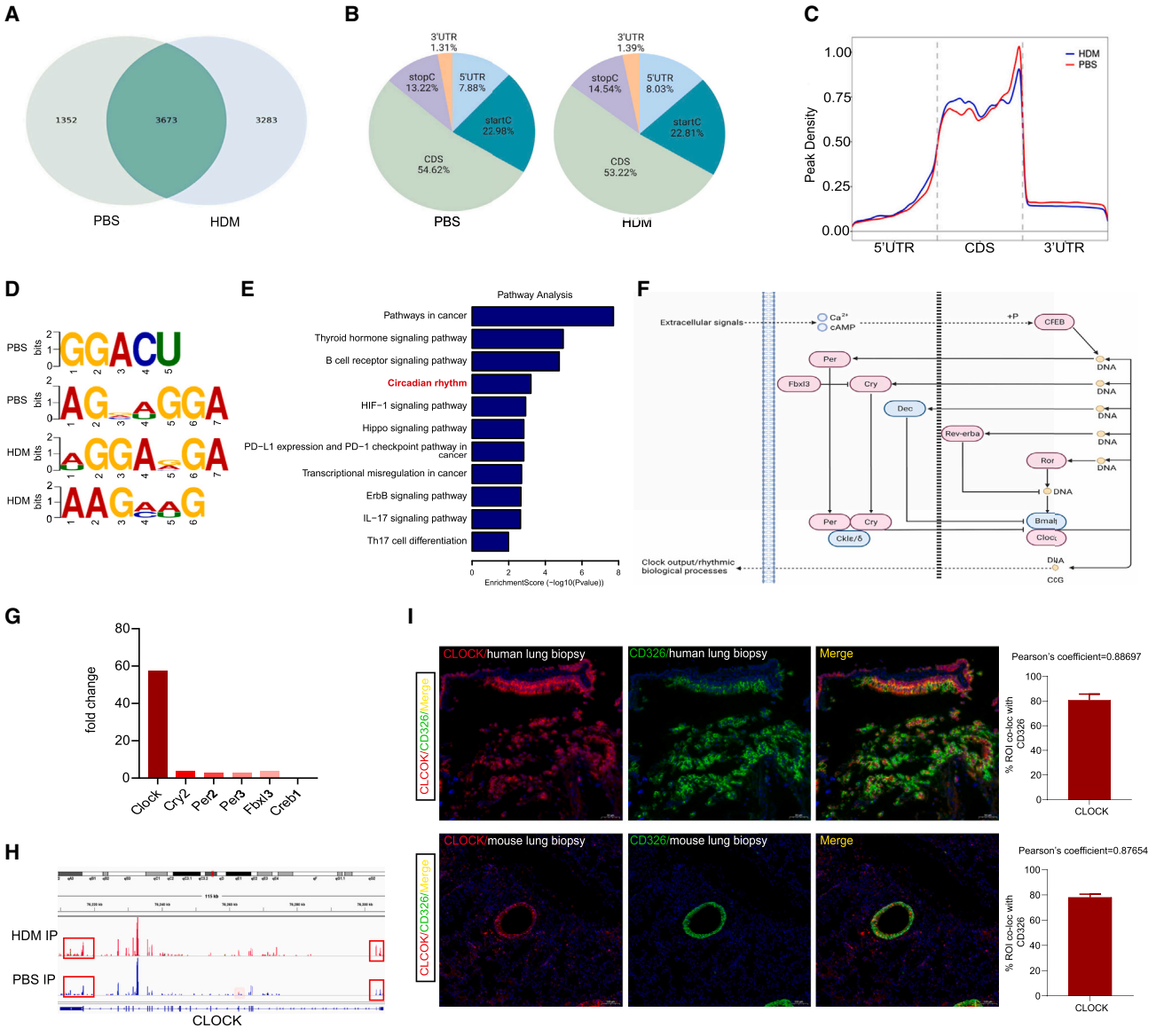

Figure 3. Widespread m6A modification and identification of important biological pathways with altered methylation in allergic mouse AECs

(A) Venn diagram of m6A-modified genes in normal and allergic AECs from C57/BL6 mouse.

(B) The distribution of m6A peaks in normal and allergic AECs from C57/BL6 mouse.

(C) The normalized distribution of m6A peaks across the start codon, CDS (coding sequence), and stop codon of mRNAs for normal and allergic C57/BL6 mouse AEC m6A peaks.

(D) The consensus motif detected by DREME (Discriminative Regular Expression Motif Elicitation) motif analysis with m6A-seq data.

(E) KEGG pathway analysis of transcripts with increased m6A methylation and upregulated mRNA expression in asthma model against normal tissues.

(F) Diagram of the circadian clock pathway with genes affected by m6A marked by red. The diagram is based on KEGG annotations.

(G) Gene fold change in allergic C57/BL6 mouse AECs.

(H) The m6A abundances on CLOCK mRNA transcripts in normal and allergic AECs from C57/BL6 mouse as detected by m6A-seq.

(I) IF staining of human and C57/BL6 mouse lung biopsy for CLOCK and CD326. Scale bars: 50 μm. AECs were obtained from 25–30 mice per group.

identified 6,956 genes in allergic mice. Among these 6,956 genes, 3,673 genes were common between the normal and allergic mice (Figure 3A), and the preferential locations of m6A on transcripts are shown in Figures 3B and 3C. We found two motifs among the top 1,000 most significant peaks representing the most common consensus in both normal and allergic mouse AEC groups (Figure 3D). KEGG pathway analyses showed that genes with elevated m6A modification in allergic mouse AECs mainly focus on pathways in cancer, the thyroid hormone signaling pathway, the B cell receptor signaling pathway, and the circadian clock signaling pathway (Figure 3E). It is characteristic of asthma that symptoms worsen overnight, particularly in

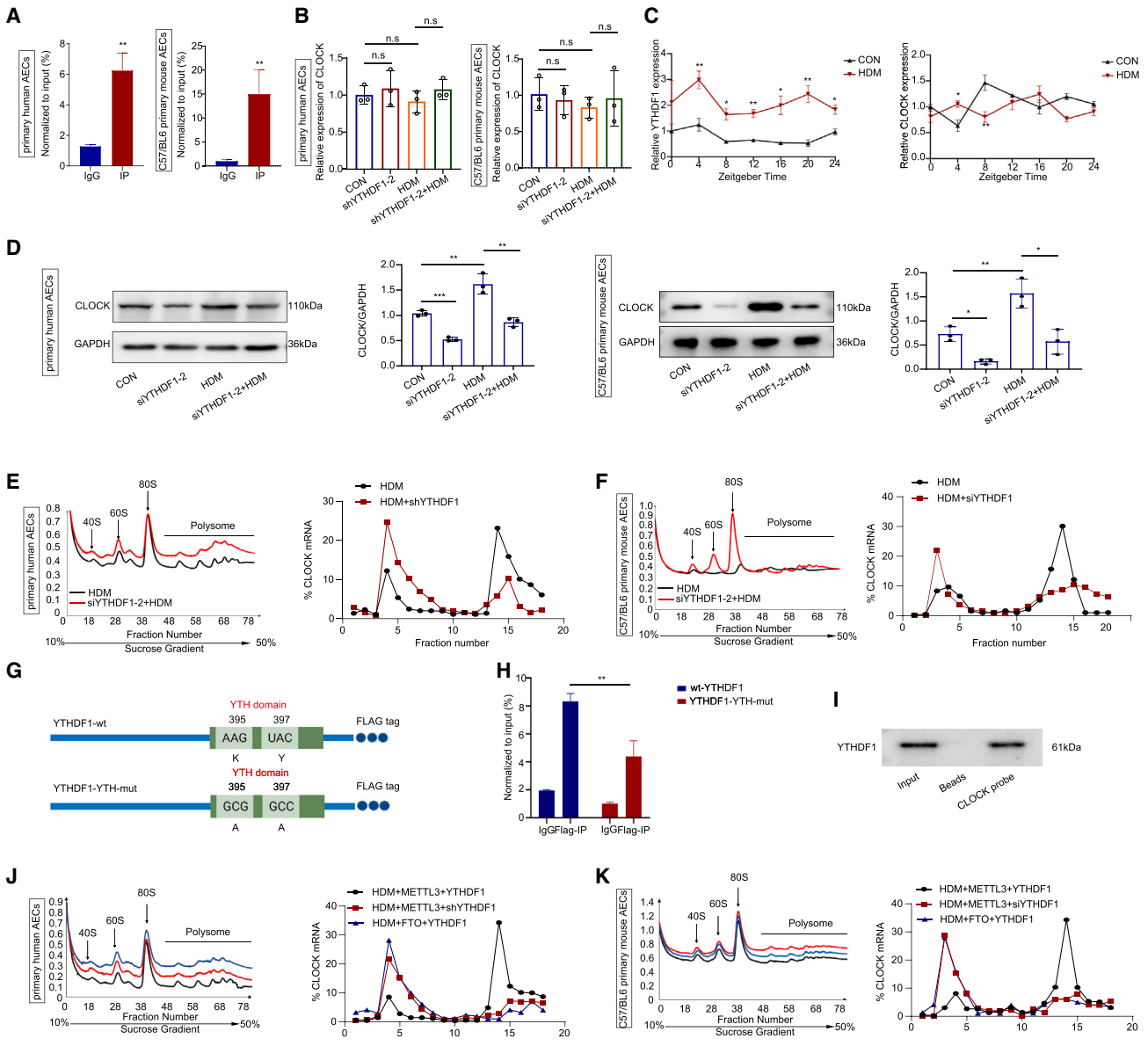

Figure 4. YTHDF1 recognizes and promotes the translation of m6A-modified CLOCK mRNA

(A) RIP-RT-qPCR analyzing of the binding of YTHDF1 protein to CLOCK mRNA in human and C57/BL6 mouse primary AECs (n = 3–4 subjects per group).

(B) RT-qPCR detecting CLOCK mRNA expression in human and C57/BL6 mouse primary AECs (n = 3–4 human subjects per group or n = 3–5 mice per group).

(C) Control and HDM-stimulated C57/BL6 mouse AECs were collected at different zeitgeber times (ZTs). Expression of YTHDF1 and CLOCK genes were determined by RT-qPCR (n = 3–5 mice per group).

(D) CLOCK protein levels were measured by immunoblot of human and C57/BL6 mouse primary AECs. Protein ratios derived from the values against GAPDH were plotted as histograms (n = 3–5 mice per group).

(E) Polysome profiling in primary human AECs; RT-qPCR analysis of CLOCK mRNA in different polysome fractions of primary human AECs is shown on the right. 18S rRNA was used as a negative control.

(F) Polysome profiling in C57/BL6 primary mouse AECs; RT-qPCR analysis of CLOCK mRNA in different polysome fractions of C57/BL6 primary mouse AECs is shown on the right. 18S rRNA was used as a negative control.

(G) Schematic representation of wild-type (YTHDF1-WT) and mutant (YTHDF1-YTH-mut) YTHDF1 constructs.

(H) RIP-derived RNA and protein in BEAS-2B were measured by RT-qPCR.

(I) RNA pull-down followed by western blotting for YTHDF1 protein BEAS-2B cell lysates incubated with synthetic CLOCK probes.

(J) Polysome profiling in primary human AECs; RT-qPCR analysis of CLOCK mRNA in different polysome fractions of primary human AECs is shown on the right.

(legend continued on next page)

the early hours of the morning, suggesting that the molecular circadian clock may play a role in the pathogenesis of asthma.[35] Therefore, circadian clock signaling pathways were further investigated. Most of the core genes in the circadian rhythm signaling pathway modified by m6A methylation were significantly upregulated in allergic mouse AECs (Figure 3F), in which the fold value of CLOCK was the highest (Figure 3G). We further analyzed the distribution of m6A peaks of CLOCK and found that the m6A abundance of CLOCK was increased in the allergic models (Figure 3H). Moreover, CLOCK was chiefly expressed in AECs of human and mouse lung tissues (Figure 3I), which was consistent with YTHDF1 characteristics. However, the other circadian rhythm genes were not found only in AECs (Figure S4N). Taken together, genes with elevated m6A modification are mainly involved in regulating the circadian rhythm signaling pathway in allergic mouse AECs.

YTHDF1 recognizes and promotes the translation of m6A-modified CLOCK mRNA

To further investigate the mechanisms underlying the capability of YTHDF1 to regulate CLOCK mRNA, we performed YTHDF1 RIP (RNA immunoprecipitation) analysis in AECs after HDM treatment. The RIP-RT-qPCR results confirmed that YTHDF1 bound to CLOCK mRNA after HDM treatment (Figures 4A and S5A). Furthermore, we examined the transcription and translation of CLOCK after YTHDF1 silencing. As expected, loss of YTHDF1 did not affect CLOCK mRNA levels (Figures 4B and S5B). Then, we harvested AECs every 4 h over a 12:12 h light-dark cycle beginning at zeitgeber time 0 (6 a.m.). We found that CLOCK expression exhibited a circadian rhythm and that HDM caused CLOCK dysregulation but did not affect its expression. In addition, YTHDF1 expression was upregulated after HDM treatment. No correlation was found between the levels of the YTHDF1 and CLOCK transcripts (Figure 4C). These results suggest that YTHDF1 did not regulate the expression of CLOCK mRNA. However, the protein abundance of CLOCK was decreased after YTHDF1 silencing (Figures 4D and S5C). We also analyzed time courses in collected lung tissues, which showed that the expression of CLOCK was reduced in *YTHDF1*$^{fl/fl}$*shh*$^{cre/+}$ mouse lung tissues at different times (Figure S5D). In addition, we observed that YTHDF1 exerted no obvious meaningful effect on the levels of other circadian rhythm proteins except for CRY2 (Figure S5E). Notably, CRY2 was not exclusively expressed in AECs (Figure S4N), which suggested that CRY2 may not be regulated only by YTHDF1. Furthermore, we found that depletion of YTHDF1 resulted in a moderate shift of CLOCK mRNA to non-polysome fractions with reduced CLOCK mRNA in translation fractions using polysome profiling, supporting that YTHDF1 regulates CLOCK protein synthesis (Figures 4E, 4F, and S5F).

To evaluate whether YTHDF1 regulating CLOCK protein expression is m6A dependent, METTL3, the most critical methyltransferase of m6A modification, was depleted in BEAS-2B cells (Figure S5G), resulting in decreased levels of CLOCK protein (Figure S5H). YTHDF1 binds m6A sites through its m6A-binding pockets located in the YTH domain. By introducing two point mutations, K395A and Y397A, in the YTH domain of YTHDF1 with a FLAG tag (YTHDF1-YTH-mut), we transfected BEAS-2B cells with the YTHDF1-WT or YTHDF1-YTH-mut construct, respectively (Figure 4G). The results revealed that CLOCK mRNA was effectively immunoprecipitated from cells transfected with YTHDF1-WT, but the interaction between YTHDF1-YTH-mut and CLOCK mRNA was not notable (Figure 4H). We also noticed that YTHDF1 protein was pulled down by the CLOCK probe (Figure 4I). In order to further clarify the regulation of CLOCK translation by YTHDF1 through m6A modification, we transfected methyltransferase METTL3 into cells and then transfected YTHDF1 and found that the translation efficiency of CLOCK was upregulated. Once the demethyltransferase FTO (obesity-associated protein) was transferred into cells and then YTHDF1 transfected, the translation efficiency of CLOCK was significantly reduced (Figures 4J, 4K, and S5I). These observations suggested that the m6A-binding pocket was crucial for YTHDF1 regulation of CLOCK mRNA. Collectively, these data indicate that YTHDF1 led to greater protein translational efficiency of the m6A-modified CLOCK.

CLOCK is a critical downstream target of YTHDF1 and participates in NLRP3 and IL-1β induction

Since YTHDF1 promotes the inflammatory response and CLOCK may be a direct target of YTHDF1, we speculated that CLOCK may play a similar role to YTHDF1 in allergic human and mouse AECs. We first measured the mRNA level of CLOCK in PBS- and HDM-treated AECs. As expected, no significant difference in the level of CLOCK mRNA expression was found between these groups (Figures 5A and S6A). However, the CLOCK protein level in the HDM group was significantly increased (Figures 5B and S6B). To further elucidate the role of CLOCK in allergic human and mouse AECs, we evaluated whether CLOCK can activate the inflammatory response to the same degree as that induced by YTHDF1. The results showed that CLOCK knockdown decreased NLRP3 and IL-1β expression in primary human AECs and BEAS-2B cells (Figures 5C, 5D, S6C, and S6D). In addition, we obtained similar results in HDM- or OVA-treated C57/BL6 or BALB/c strain primary mouse AECs, indicating that CLOCK's regulation of inflammation is not dependent on strains and allergens (Figures 5E, 5F, and S6E–S6G). Conversely, CLOCK overexpression activated NLRP3 and IL-1β expression (Figures S6H–S6M). However, under- and overexpression of CLOCK did not affect the expression of TSLP, IL-25, or IL-33, respectively (Figures S6N and S6O). Next, we also observed that knockdown of CLOCK in YTHDF1-overexpressing AECs weakened the proinflammatory effect of YTHDF1, primarily by abolishing

(K) Polysome profiling in C57/BL6 primary mouse AECs; RT-qPCR analysis of CLOCK mRNA in different polysome fractions of C57/BL6 primary mouse AECs is shown on the right. 18S rRNA was used as a negative control.

Data are shown as the mean ± SEM and are representative of three independent experiments. *$p < 0.05$, **$p < 0.01$, ***$p < 0.001$, and ****$p < 0.0001$; n.s., no statistical significance. Student's t test in (A), one-way ANOVA with Dunnett's multiple comparison test in (B)–(D) and (I), and two-way ANOVA with Tukey's test in (H).

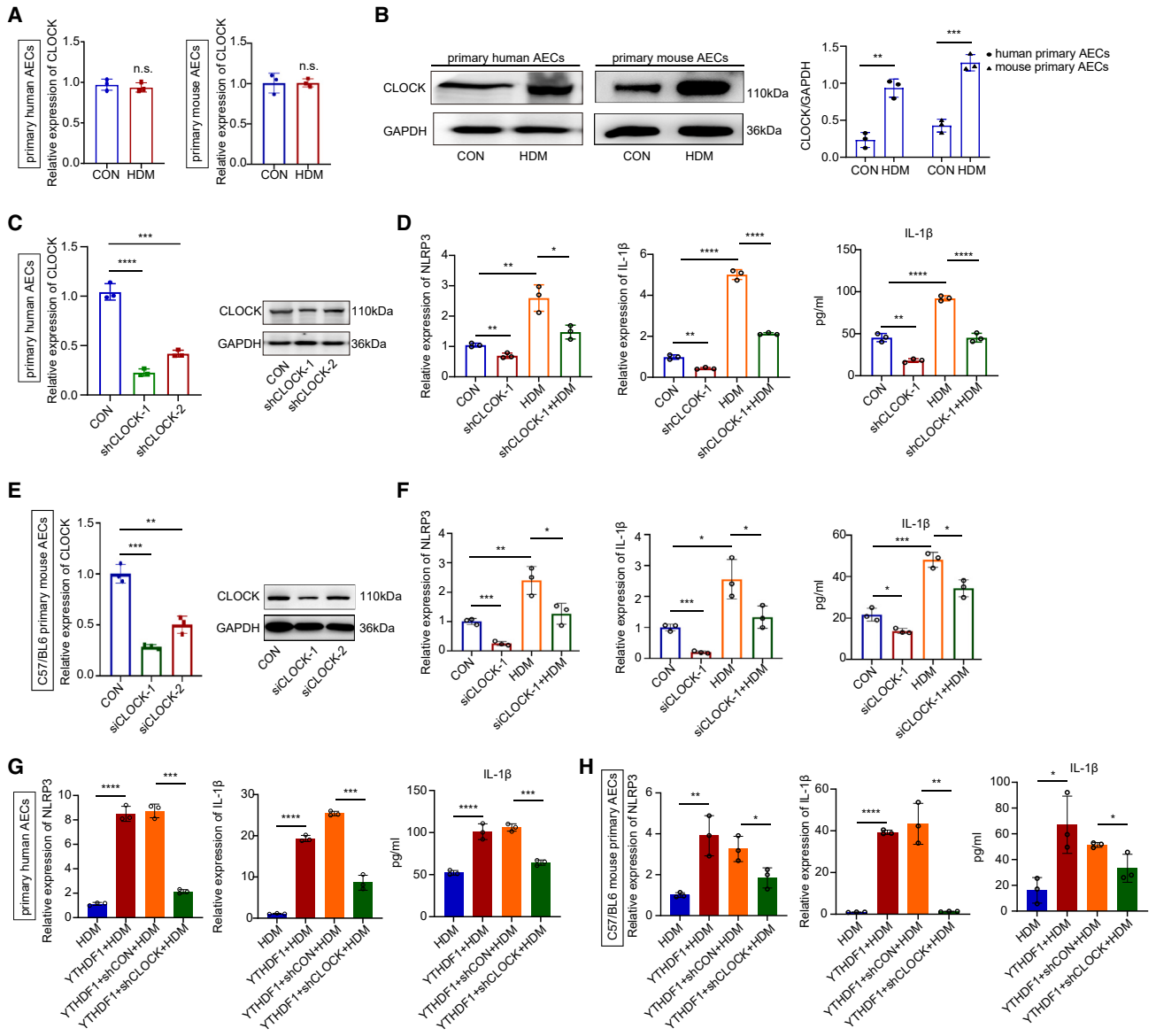

Figure 5. CLOCK is a critical downstream target of YTHDF1 and participates in NLRP3 inflammasome and IL-1β induction

(A) RT-qPCR measuring mRNA expression of CLOCK in primary human and C57/BL6 mouse AECs (n = 3–4 subjects per group or n = 3–5 mice per group).

(B) Immunoblot analyzing the levels of CLOCK in primary human and C57/BL6 mouse AECs. Protein ratios derived from the values against GAPDH were plotted as histograms (n = 3–4 subjects per group or n = 3–5 mice per group).

(C) RT-qPCR and immunoblots detecting the effect of siCLOCK on primary human AECs (n = 3–4 subjects per group).

(D) RT-qPCR detecting the expression of NLRP3 and IL-1β in primary human AECs and ELISA analyzing concentrations of IL-1β in primary human AEC supernatants (n = 3–4 subjects per group).

(E) RT-qPCR and immunoblots detecting the effect of siCLOCK on C57/BL6 primary mouse AECs (n = 3–5 mice per group).

(F) RT-qPCR detecting the expression of NLRP3 and IL-1β in HDM-stimulated C57/BL6 primary mouse AECs and ELISA analyzing concentrations of IL-1β in C57/BL6 primary mouse AEC supernatants (n = 3–5 mice per group).

(G and H) Construction of stable overexpression YTHDF1 primary human AECs and C57/BL6 mouse AECs with shCLOCK constructs, RT-qPCR detecting the expression of NLRP3 and IL-1β, and ELISA analyzing concentrations of IL-1β in primary human and C57/BL6 mouse AECs supernatants (n = 3–4 subjects per group or n = 3–5 mice per group).

Data are shown as the mean ± SEM and are representative of three independent experiments. *p < 0.05, **p < 0.01, ***p < 0.001, and ****p < 0.0001; n.s., no statistical significance. Student's t test in (A) and one-way ANOVA with Dunnett's multiple comparison test in (B)–(J).

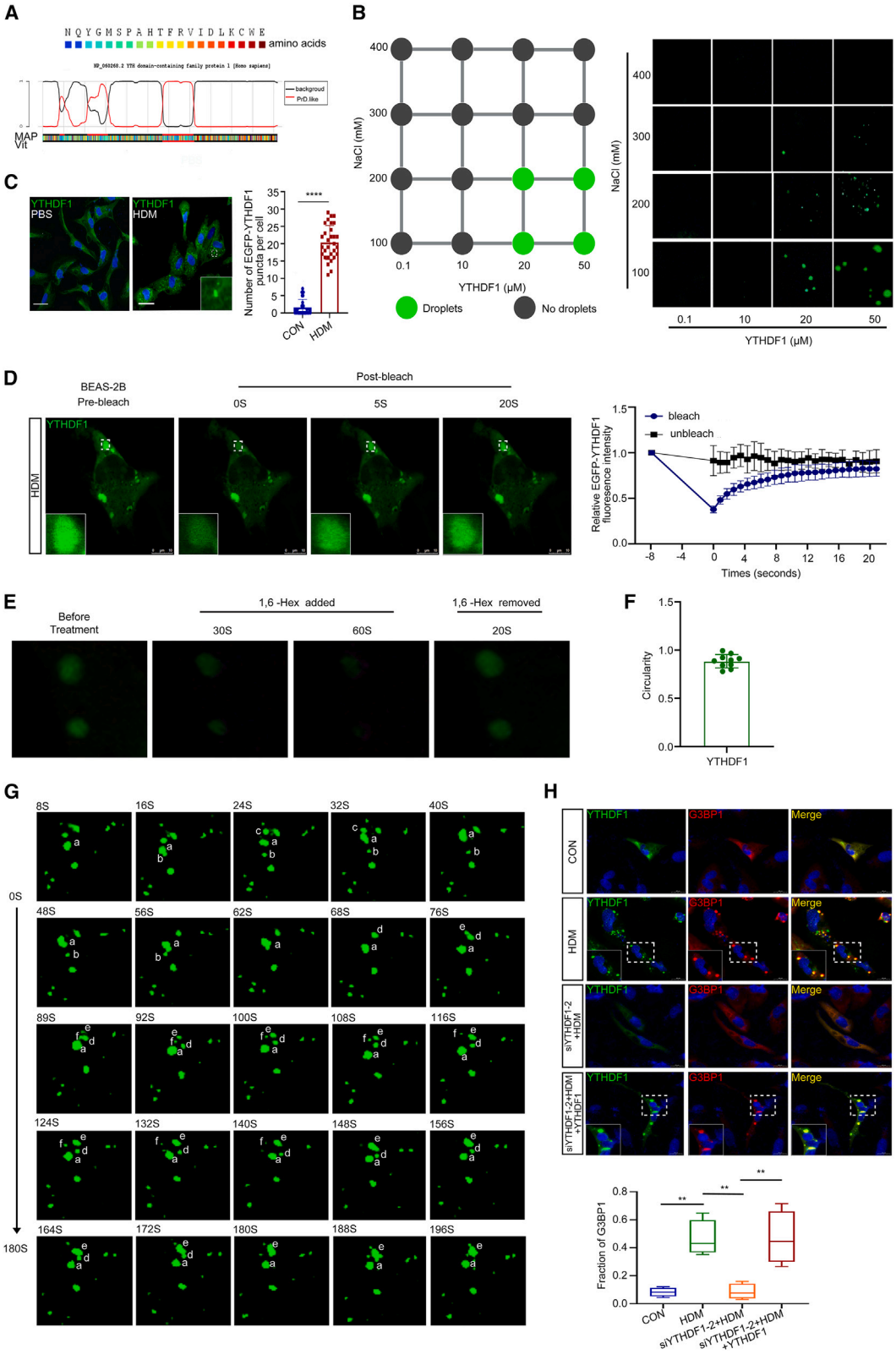

(legend on next page)

NLRP3 and IL-1β expression (Figures 5G, 5H, and S6P). Taken together, these analyses indicate that CLOCK is a critical downstream target of YTHDF1 that facilitates NLRP3 and IL-1β expression in allergic airway inflammation.

HDM triggers LLPS of YTHDF1

Previous studies have shown that YTHDF1 recruits m6A-mRNAs to SGs through condensate formation mediated by LLPS in the cytoplasm.[36] We evaluated whether YTHDF1 participates in CLOCK regulation through phase separation in allergic BEAS-2B cells. First, we revealed that YTHDF1 carries a prion-like domain (PrLD) and multiple disordered sequences (Figure 6A), which were found to be drivers of LLPS.[37] Purified YTHDF1 formed spherical droplets *in vitro*, and YTHDF1 LLPS was enhanced by increasing the protein concentration but was dampened by treatment with salt (Figure 6B). Furthermore, YTHDF1-EGFP (enhanced green fluorescent protein) phase separation was significantly higher in HDM-stimulated BEAS-2B cells (Figure 6C). By performing fluorescence recovery after photobleaching to assess the dynamics of droplet formation, we found that fluorescence in foci labeled with YTHDF1-EGFP recovered after bleaching (Figure 6D). After being incubated with 1,6-hexanediol, YTHDF1 puncta were rapidly dissolved but reformed shortly after the removal of 1,6-hexanediol (Figure 6E), and the circularity of phase separated YTHDF1 is nearly 1 (Figure 6F). Moreover, YTHDF1 formed round condensates, which underwent fusion and separation in HDM-treated BEAS-2B cells (Figures 6G; Video S1). These results indicate that YTHDF1 underwent LLPS after HDM stimulation. Since m6A-binding proteins play an important role in SG formation,[36] we next examined the roles of YTHDF1 in SG assembly. We observed strong colocalization of endogenous YTHDF1 proteins with SGs. Notably, after HDM challenge, SG formation was substantially increased, knockdown of YTHDF1 abolished the formation of SGs, and reintroducing YTHDF1 into the knockdown cells rescued the SG formation (Figure 6H). These results suggest that YTHDF1 LLPS was enhanced under HDM stimulation and participated in the SG formation. Collectively, these results suggest that YTHDF1 is involved in the regulation of downstream target gene expression in SGs.

YTHDF1 LLPS is essential for CLOCK translation and the inflammatory response

Given that CLOCK is a downstream target gene of YTHDF1 and that YTHDF1 is stimulated by HDM to induce LLPS, we sought to explore whether YTHDF1 is involved in regulating CLOCK through LLPS. Colocalization of CLOCK mRNA with YTHDF1 granules and Ras-GTPase-activating protein-binding protein 1 showed that YTHDF1 bound to its target during condensate formation in SGs, while CLOCK mRNA was randomly distributed in the cytoplasm in YTHDF1-knockdown BEAS-2B cells (Figure 7A), confirming that CLOCK mRNA was located in YTHDF1 granules and that this translocation was mediated by YTHDF1. We speculated as to whether YTHDF1 depends on LLPS to regulate CLOCK translation. Therefore, we constructed YTHDF1-C fragments that carried neither the intrinsically disordered regions (IDRs) nor PrLDs (Figure 7B). As expected, YTHDF1-C fragments did not induce LLPS (Figures S7A and S7B). We used a translating RNA imaging by coat protein knockoff reporter system to determine whether LLPS of YTHDF1 is required for the translation of CLOCK. NLS-PCP-GFP (a PP7 coat protein fused to a nuclear localization sequence [NLS] and GFP) and NLS-MCP-RFP (an MS2 coat protein fused to an NLS and red fluorescent protein [RFP]) resulted in two-color labeling of nuclear CLOCK mRNA in transfected BEAS-2B cells. Coexpression of blue fluorescent protein (BFP)-tagged YTHDF1 yielded a fraction of CLOCK into YTHDF1 granules (blue) in the cytoplasm. CLOCK mRNA in YTHDF1 granules was labeled with RFP but not GFP, indicative of the translated state. Coexpression of BFP-YTHDF1-C led to the recruitment of CLOCK mRNA in the cytoplasm, but the CLOCK mRNA was untranslated, as this system was labeled with both RFP and GFP. These data support that LLPS is essential for YTHDF1-mediated CLOCK translation (Figure 7C).

We showed earlier that YTHDF1 regulates CLOCK and is mainly involved in promoting NLRP3 and IL-1β expression. We supposed that YTHDF1 depends on its LLPS ability to activate NLRP3 and IL-1β expression. YTHDF1-C fragments did induce

Figure 6. HDM triggers LLPS of YTHDF1

(A) The color-coded schematic representation of the aligned amino acid sequence and corresponding prion-like domain disorder propensity plots (red and black traces) for YTHDF1 generated using the PLAAC (prion-like amino acid composition) tool. The y axis of the plot represents prion-like regions (1) and regions of background amino acid composition (0).

(B) LLPS of purified recombinant YTHDF1 at various amounts and with increasing NaCl under 10% PEG. Left, summary of phase separation behavior of YTHDF1; right, representative fluorescent microscopy images.

(C) Laser confocal detection of YTHDF1 in BEAS-2B transfected with YTHDF1-EGFP. Scale bars: 20 μm. Quantification of the number of YTHDF1 puncta per cell (n = 30).

(D) Fluorescence recovery after photobleaching (FRAP) of partially photobleached YTHDF1-EGFP foci in YTHDF1-overexpressed BEAS-2B. Scale bars: 10 μm. The line traces represent mean fractional fluorescence (unbleached n = 3; bleached n = 3).

(E) YTHDF1-GFP droplets were disrupted by 10% 1,6-hexanediol and recovered after removal of 1,6-hexanediol.

(F) The circularity of phase-separated YTHDF1 in BEAS-2B (n = 10 puncta).

(G) Live-cell images showing the fusion and separation of YTHDF1-EGFP granules in transfected BEAS-2B.

(H) IF and laser confocal microscopy detection of colocalization of YTHDF1 and Ras-GTPase-activating protein (GAP)-binding protein 1 (G3BP1) in BEAS-2B. Scale bars: 20 μm. Quantification of the fraction of G3BP1 in cells was plotted as histograms (CON: n = 230 cells, HDM: n = 245 cells, siYTHDF1+HDM, n = 162 cells, siYTHDF1+HDM+YTHDF1: n = 222 cells).

Data are shown as the mean ± SEM and are representative of three independent experiments. **$p < 0.01$ and ****$p < 0.0001$. Student's t test in (C). The boxplots show the median (middle lines) and 25%–75% quartiles (boxes), and Tukey-style whiskers extend to the most extreme datapoint within 1.5× interquartile ranges (IQRs) beyond the box. p values were determined by unpaired Mann-Whitney U test, two-sided in (H).

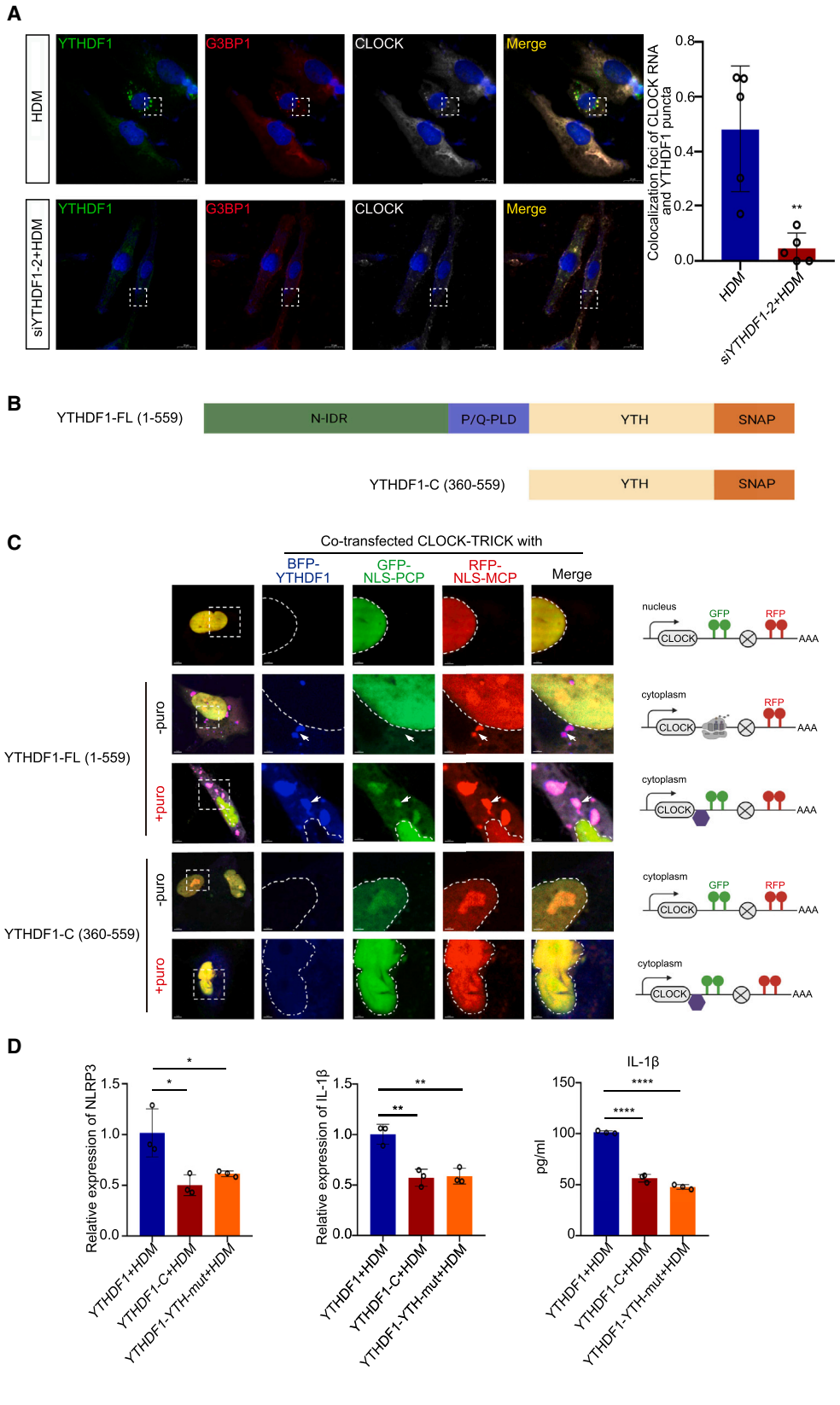

(legend on next page)

a decrease in NLRP3 and IL-1β expression. Moreover, YTHDF1-YTH fragments also suppressed NLRP3 and IL-1β expression (Figure 7D). These results suggest that both the N-terminal IDRs and PrLDs and the C-terminal YTH domain are functionally required for NLRP3 and IL-1β expression.

DISCUSSION

m6A is the most prevalent internal modification of mammalian messenger RNA[11,38] and plays essential roles in normal biological processes and development by regulating the fate of target RNAs.[39,40] Thus far, very limited studies have focused on the role of m6A modification in allergic airway inflammation. In the present study, we observed an increased tendency of METTL3 and YTHDF1 in allergic AECs, including primary human and mouse AECs and the BEAS-2B cells. Thus, m6A modifications seem to be critical to AECs in allergic airway inflammation.

In this study, we focused on the YTHDF1 role in allergic airway inflammation. YTHDF1, as a reader of m6A modifications, has been reported to be activated in various physiological and pathological processes,[17,34,41,42] but the clinical significance, molecular mechanisms, and role of YTHDF1 in allergic airway inflammation remain to be investigated. To verify the clinical significance of YTHDF1, we also collected and analyzed clinical bronchofiberscope brush biopsy specimens showing that YTHDF1 was expressed mainly in AECs and significantly increased in asthmatic patients. In addition, YTHDF1 expression was correlated with the FEV_1 value. These findings suggest that YTHDF1 may be an effective biomarker of allergic airway inflammation. At the same time, the level of METTL3 mRNA in asthmatic patients revealed a significant upward trend. Hence, METTL3 may be another potential biomarker that requires further exploration in future research. Additionally, highly expressed YTHDF1 facilitated the inflammatory response. Previous literature reported that YTHDF1 could directly promote the translation of inflammasome NLRP3 in endogenous epithelial cells stimulated by endotoxin and that YTHDF1 alleviated sepsis by inducing NLRP3 ubiquitination to inhibit caspase-1-dependent pyroptosis.[43,44] However, no changes in NLRP3 m6A modification were detected in our m6A-seq data after allergen stimulation, suggesting that m6A modification in AECs stimulated by allergens may regulate inflammatory responses through other pathways. The m6A-seq analysis provided an initial roadmap leading to the discovery of m6A functions in allergic mouse AECs. We screened methylated genes and found them to be mainly enriched in the biological circadian rhythm pathway. Recent findings have indicated that circadian clock proteins, notably CLOCK, BMAL1, and REV-ERBα, can impact immune cell function, host defense, and inflammation.[45–47] Regarding the involvement of REV-ERBα in regulating inflammasome NLRP3 in various diseases, such as Parkinson's disease and colon inflammation, there is still relatively limited research on the involvement of the CLOCK gene in regulating inflammasome NLRP3.[48–50] The emerging concept suggests that time of day is critical to the nature of the immune response and that its dysregulation may lead to inflammatory diseases or immunodeficiency.[51,52] In this study, we found that YTHDF1 mainly regulates CLOCK protein translation efficiency in an m6A-modification-dependent manner. Moreover, CLOCK, as a downstream target gene of YTHDF1, is mainly involved in regulating NLRP3 and IL-1β but not TSLP, IL-25, or IL-33. Thus, these data suggest that YTHDF1, an RNA-binding protein, is involved in regulating the generation of NLRP3 and IL-1β, which promote the airway inflammatory response through CLOCK. Importantly, to determine whether our findings were dependent on the mouse strains or allergens, we stimulated C57/BL6 or BALB/c mouse primary AECs with HDM or OVA and found that the expression of YTHDF1 was promoted and the levels of NLRP3, IL-1β, TSLP, IL-25, and IL-33 were increased. CLOCK was implicated in regulating the expression of NLRP3 and IL-1β. These results indicate that our findings were not strain or allergen dependent. However, we have not investigated how YTHDF1 affects the levels of TSLP, IL-25, and IL-33 in this work; further investigation is needed to elaborate the relevant detailed mechanisms.

Studies have proven that LLPS is a physical property of the YTHDF1 protein. Different stimuli, including heat shock, sodium arsenite, and endoplasmic reticulum stress, lead to LLPS in the YTHDF1-3 protein.[29] The mechanism behind this has not been fully elucidated. Recent literature has reported that arsenite promotes YTHDF2 LLPS by activating the oxidative stress mechanism. In addition, studies have demonstrated that airway inflammation induced by allergens can also promote oxidative stress, suggesting that HDM-induced LLPS involving YTHDF1 may also be due to the promotion of oxidative stress mechanisms. In addition, accumulating evidence has shown that the coacervates formed by LLPS are involved in multiple critical cellular activities, including gene expression, assembly of signaling clusters, and so on. This also suggests that AECs stimulated by allergens promote an increase in YTHDF1 gene and protein expression leading to the intracellular accumulation and formation of LLPS. Our mechanistic studies revealed that the HDM-stimulated YTHDF1 protein undergoes LLPS to form granules, recruiting CLOCK mRNA into the granules and participating in regulating CLOCK translation. The YTHDF1-C's proinflammatory potential was

Figure 7. Quantity of YTHDF1-binding CLOCK is enriched in SGs after HDM treatment and LLPS of YTHDF1 is required for inflammatory response

(A) Laser confocal detection of CLOCK mRNA by fluorescence *in situ* hybridization (FISH) and YTHDF1 by IF and DAPI in BEAS-2B. Quantitative summary of colocalization of total CLOCK mRNA with YTHDF1 puncta. Data are shown as n = 50 cells (HDM) and n = 50 cells (HDM+siYTHDF1).

(B) Truncated YTHDF1 constructs tagged with SNAP at the C-terminal end.

(C) Live-cell imaging analysis of the effect of YTHDF1-WT or YTHDF1-C mutants on CLOCK translation using the TRICK (translating RNA imaging by coat protein knockoff) reporter system in cotransfected BEAS-2B cells.

(D) RT-qPCR detecting the expression of NLRP3 and IL-1β in BEAS-2B and ELISA analyzing the concentrations of IL-1β in BEAS-2B supernatant.

Data are shown as the mean ± SEM and are representative of three independent experiments. *$p < 0.05$, **$p < 0.01$, and ****$p < 0.0001$. Student's t test in (A) and one-way ANOVA with Dunnett's multiple comparison test in (D).

greatly weakened by decreasing its effect on NLRP3 and IL-1β expression. In addition, YTHDF1-YTH mutations led to reduced NLRP3 and IL-1β expression. Based on our previous findings, LLPS of YTHDF1 recruits downstream target CLOCK mRNA and binds to the YTH domain and then participates in regulating inflammatory response through the generation of NLRP3 and IL-1β.

In summary, our study delineates a YTHDF1-m6A module that regulates the CLOCK function, which has implications for enhancing NLRP3 and IL-1β expression in allergic airway inflammation. These results suggest that m6A modification plays a critical role in allergic airway inflammation. Additionally, the m6A modification of CLOCK might underlie a general epigenetics regulatory mechanism affecting a range of other biological processes and hence warrants further exploration.

Limitations of the study

Our study reveals that YTHDF1 promotes the expression of NLRP3 and IL-1 through the target gene CLOCK, thereby stimulating inflammatory response. However, YTHDF1 promotes inflammatory response through not only upregulating NLRP3 and IL-1β but also activating the expression of TSLP, IL-25, and IL-33. This may be potentially due to YTHDF1 action through other downstream target genes, which needs to be further explored. In addition, although we used a variety of cell types and animal models, the role of YTHDF1 in allergic diseases with more clinically related tissues or cells, such as patient-derived tracheas and AECs as well as additional animal models, still needs to be inferred. In terms of allergens, all experimental models bear some inherent deficiency, such as the potential contaminant compositions in OVA, and other allergens with different features from OVA or HDM may be tested. Finally, the number of subjects was not very large; it would be critical to gain a deeper understanding of molecular mechanisms in an increased cohort of patients.

STAR★METHODS

Detailed methods are provided in the online version of this paper and include the following:

SUPPLEMENTAL INFORMATION

Supplemental information can be found online at https://doi.org/10.1016/j.celrep.2024.113947.

ACKNOWLEDGMENTS

The authors thank the staff of the Research Center for Experimental Medicine of Ruijin Hospital affiliated with Shanghai Jiao Tong University School of Medicine. This study was supported by the National Natural Science Foundation of China (grant nos.91542202, 81970021, and 82170035 to Z.X., 82300037 to J. Wang, and 81900015 to J.L.) and the Innovative Research Team of High-level Local Universities in Shanghai (grant to Z.X.). This study is also supported by funds from National Key Research Project of MOST (2023YFA0915000 to M.W.) and the Wenzhou Institute University of Chinese Academy of Sciences (J.S. and M.W.).

AUTHOR CONTRIBUTIONS

J. Wang, Y.Z., and M.Z. performed experiments; Z.X. and J. Wang designed the experiments; J.L., W.T., Y.W., Q.W., W.S., and M.X. provided human patient samples and animal models; M.Z. conducted the bioinformatics analysis; J. Wang, M.W., and J.S. performed critical reading/editing of the manuscript; J. Wang wrote the manuscript; and Z.X. supervised the study. All authors participated in data interpretation.

DECLARATION OF INTERESTS

The authors declare no competing interests.

Received: July 21, 2023
Revised: January 23, 2024
Accepted: February 27, 2024

REFERENCES

1. Maciag, M.C., and Phipatanakul, W. (2020). Prevention of Asthma: Targets for Intervention. Chest *158*, 913–922. https://doi.org/10.1016/j.chest.2020.04.011.
2. Corso-Díaz, X., Jaeger, C., Chaitankar, V., and Swaroop, A. (2018). Epigenetic control of gene regulation during development and disease: A view from the retina. Prog. Retin. Eye Res. *65*, 1–27. https://doi.org/10.1016/j.preteyeres.2018.03.002.
3. Agustí, A., Melén, E., DeMeo, D.L., Breyer-Kohansal, R., and Faner, R. (2022). Pathogenesis of chronic obstructive pulmonary disease: understanding the contributions of gene-environment interactions across the lifespan. Lancet. Respir. Med. *10*, 512–524. https://doi.org/10.1016/S2213-2600(21)00555-5.
4. Noble, A.J., Nowak, J.K., Adams, A.T., Uhlig, H.H., and Satsangi, J. (2023). Defining Interactions Between the Genome, Epigenome, and the Environment in Inflammatory Bowel Disease: Progress and Prospects. Gastroenterology *165*, 44–60.e2. https://doi.org/10.1053/j.gastro.2023.03.238.

5. Nejati-Koshki, K., Roberts, C.T., Babaei, G., and Rastegar, M. (2023). The Epigenetic Reader Methyl-CpG-Binding Protein 2 (MeCP2) Is an Emerging Oncogene in Cancer Biology. Cancers *15*, 2683. https://doi.org/10.3390/cancers15102683.

6. Ntontsi, P., Photiades, A., Zervas, E., Xanthou, G., and Samitas, K. (2021). Genetics and Epigenetics in Asthma. Int. J. Mol. Sci. *22*, 2412. https://doi.org/10.3390/ijms22052412.

7. Stikker, B.S., Hendriks, R.W., and Stadhouders, R. (2023). Decoding the genetic and epigenetic basis of asthma. Allergy *78*, 940–956. https://doi.org/10.1111/all.15666.

8. Teng, P.C., Liang, Y., Yarmishyn, A.A., Hsiao, Y.J., Lin, T.Y., Lin, T.W., Teng, Y.C., Yang, Y.P., Wang, M.L., Chien, C.S., et al. (2021). RNA Modifications and Epigenetics in Modulation of Lung Cancer and Pulmonary Diseases. Int. J. Mol. Sci. *22*, 10592. https://doi.org/10.3390/ijms221910592.

9. Gruhn, W.H., Tang, W.W.C., Dietmann, S., Alves-Lopes, J.P., Penfold, C.A., Wong, F.C.K., Ramakrishna, N.B., and Surani, M.A. (2023). Epigenetic resetting in the human germ line entails histone modification remodeling. Sci. Adv. *9*, eade1257. https://doi.org/10.1126/sciadv.ade1257.

10. Messingschlager, M., Bartel-Steinbach, M., Mackowiak, S.D., Denkena, J., Bieg, M., Klös, M., Seegebarth, A., Straff, W., Süring, K., Ishaque, N., et al. (2023). Genome-wide DNA methylation sequencing identifies epigenetic perturbations in the upper airways under long-term exposure to moderate levels of ambient air pollution. Environ. Res. *233*, 116413. https://doi.org/10.1016/j.envres.2023.116413.

11. Sendinc, E., and Shi, Y. (2023). RNA m6A methylation across the transcriptome. Mol. Cell *83*, 428–441. https://doi.org/10.1016/j.molcel.2023.01.006.

12. Zhuang, H., Yu, B., Tao, D., Xu, X., Xu, Y., Wang, J., Jiao, Y., and Wang, L. (2023). The role of m6A methylation in therapy resistance in cancer. Mol. Cancer *22*, 91. https://doi.org/10.1186/s12943-023-01782-2.

13. Wendt, L., Pickin, M.J., Bodmer, B.S., Reiche, S., Feneant, L., Holper, J.E., Fuchs, W., Groseth, A., and Hoenen, T. (2023). N(6)-methyladenosine is required for efficient RNA synthesis of Ebola virus and other haemorrhagic fever viruses. Emerg Microbes Infect *12*, 2223732. https://doi.org/10.1080/22221751.2023.2223732.

14. Feng, Y., Yuan, P., Guo, H., Gu, L., Yang, Z., Wang, J., Zhu, W., Zhang, Q., Cao, J., Wang, L., and Jiao, Y. (2023). METTL3 Mediates Epithelial-Mesenchymal Transition by Modulating FOXO1 mRNA N(6) -Methyladenosine-Dependent YTHDF2 Binding: A Novel Mechanism of Radiation-Induced Lung Injury. Adv. Sci. *10*, e2204784. https://doi.org/10.1002/advs.202204784.

15. Chen, M., Wei, L., Law, C.T., Tsang, F.H.C., Shen, J., Cheng, C.L.H., Tsang, L.H., Ho, D.W.H., Chiu, D.K.C., Lee, J.M.F., et al. (2018). RNA N6-methyladenosine methyltransferase-like 3 promotes liver cancer progression through YTHDF2-dependent posttranscriptional silencing of SOCS2. Hepatology *67*, 2254–2270. https://doi.org/10.1002/hep.29683.

16. Shi, H., Wang, X., Lu, Z., Zhao, B.S., Ma, H., Hsu, P.J., Liu, C., and He, C. (2017). YTHDF3 facilitates translation and decay of N(6)-methyladenosine-modified RNA. Cell Res. *27*, 315–328. https://doi.org/10.1038/cr.2017.15.

17. Hu, L., Wang, J., Huang, H., Yu, Y., Ding, J., Yu, Y., Li, K., Wei, D., Ye, Q., Wang, F., et al. (2021). YTHDF1 Regulates Pulmonary Hypertension through Translational Control of MAGED1. Am. J. Respir. Crit. Care Med. *203*, 1158–1172. https://doi.org/10.1164/rccm.202009-3419OC.

18. Li, S., Qi, Y., Yu, J., Hao, Y., He, B., Zhang, M., Dai, Z., Jiang, T., Li, S., Huang, F., et al. (2022). Nuclear Aurora kinase A switches m(6)A reader YTHDC1 to enhance an oncogenic RNA splicing of tumor suppressor RBM4. Signal Transduct Target Ther *7*, 97. https://doi.org/10.1038/s41392-022-00905-3.

19. Liu, T., Wei, Q., Jin, J., Luo, Q., Liu, Y., Yang, Y., Cheng, C., Li, L., Pi, J., Si, Y., et al. (2020). The m6A reader YTHDF1 promotes ovarian cancer progression via augmenting EIF3C translation. Nucleic Acids Res. *48*, 3816–3831. https://doi.org/10.1093/nar/gkaa048.

20. Yan, S., Zhou, X., Wu, C., Gao, Y., Qian, Y., Hou, J., Xie, R., Han, B., Chen, Z., Wei, S., and Gao, X. (2023). Adipocyte YTH N(6)-methyladenosine RNA-binding protein 1 protects against obesity by promoting white adipose tissue beiging in male mice. Nat. Commun. *14*, 1379. https://doi.org/10.1038/s41467-023-37100-z.

21. Luo, X., Cao, M., Gao, F., and He, X. (2021). YTHDF1 promotes hepatocellular carcinoma progression via activating PI3K/AKT/mTOR signaling pathway and inducing epithelial-mesenchymal transition. Exp. Hematol. Oncol. *10*, 35. https://doi.org/10.1186/s40164-021-00227-0.

22. Bai, X., Wong, C.C., Pan, Y., Chen, H., Liu, W., Zhai, J., Kang, W., Shi, Y., Yamamoto, M., Tsukamoto, T., et al. (2022). Loss of YTHDF1 in gastric tumors restores sensitivity to antitumor immunity by recruiting mature dendritic cells. J Immunother Cancer *10*. https://doi.org/10.1136/jitc-2021-003663.

23. Protter, D.S.W., and Parker, R. (2016). Principles and Properties of Stress Granules. Trends Cell Biol. *26*, 668–679. https://doi.org/10.1016/j.tcb.2016.05.004.

24. Yang, P., Mathieu, C., Kolaitis, R.M., Zhang, P., Messing, J., Yurtsever, U., Yang, Z., Wu, J., Li, Y., Pan, Q., et al. (2020). G3BP1 Is a Tunable Switch that Triggers Phase Separation to Assemble Stress Granules. Cell *181*, 325–345.e28. https://doi.org/10.1016/j.cell.2020.03.046.

25. Al-Husini, N., Tomares, D.T., Bitar, O., Childers, W.S., and Schrader, J.M. (2018). alpha-Proteobacterial RNA Degradosomes Assemble Liquid-Liquid Phase-Separated RNP Bodies. Mol. Cell *71*, 1027–1039.e1014. https://doi.org/10.1016/j.molcel.2018.08.003.

26. Jain, S., Wheeler, J.R., Walters, R.W., Agrawal, A., Barsic, A., and Parker, R. (2016). ATPase-Modulated Stress Granules Contain a Diverse Proteome and Substructure. Cell *164*, 487–498. https://doi.org/10.1016/j.cell.2015.12.038.

27. Markmiller, S., Soltanieh, S., Server, K.L., Mak, R., Jin, W., Fang, M.Y., Luo, E.C., Krach, F., Yang, D., Sen, A., et al. (2018). Context-Dependent and Disease-Specific Diversity in Protein Interactions within Stress Granules. Cell *172*, 590–604.e13. https://doi.org/10.1016/j.cell.2017.12.032.

28. Li, A., Chen, Y.S., Ping, X.L., Yang, X., Xiao, W., Yang, Y., Sun, H.Y., Zhu, Q., Baidya, P., Wang, X., et al. (2017). Cytoplasmic m(6)A reader YTHDF3 promotes mRNA translation. Cell Res. *27*, 444–447. https://doi.org/10.1038/cr.2017.10.

29. Ries, R.J., Zaccara, S., Klein, P., Olarerin-George, A., Namkoong, S., Pickering, B.F., Patil, D.P., Kwak, H., Lee, J.H., and Jaffrey, S.R. (2019). m(6)A enhances the phase separation potential of mRNA. Nature *571*, 424–428. https://doi.org/10.1038/s41586-019-1374-1.

30. Gao, Y., Pei, G., Li, D., Li, R., Shao, Y., Zhang, Q.C., and Li, P. (2019). Multivalent m(6)A motifs promote phase separation of YTHDF proteins. Cell Res. *29*, 767–769. https://doi.org/10.1038/s41422-019-0210-3.

31. Zong, X., Xiao, X., Shen, B., Jiang, Q., Wang, H., Lu, Z., Wang, F., Jin, M., Min, J., Wang, F., and Wang, Y. (2021). The N6-methyladenosine RNA-binding protein YTHDF1 modulates the translation of TRAF6 to mediate the intestinal immune response. Nucleic Acids Res. *49*, 5537–5552. https://doi.org/10.1093/nar/gkab343.

32. Shi, H., Chai, P., Jia, R., and Fan, X. (2020). Novel insight into the regulatory roles of diverse RNA modifications: Re-defining the bridge between transcription and translation. Mol. Cancer *19*, 78. https://doi.org/10.1186/s12943-020-01194-6.

33. Fang, H., Sun, Q., Zhou, J., Zhang, H., Song, Q., Zhang, H., Yu, G., Guo, Y., Huang, C., Mou, Y., et al. (2023). m(6)A methylation reader IGF2BP2 activates endothelial cells to promote angiogenesis and metastasis of lung adenocarcinoma. Mol. Cancer *22*, 99. https://doi.org/10.1186/s12943-023-01791-1.

34. Sikorski, V., Selberg, S., Lalowski, M., Karelson, M., and Kankuri, E. (2023). The structure and function of YTHDF epitranscriptomic m(6)A readers. Trends Pharmacol. Sci. *44*, 335–353. https://doi.org/10.1016/j.tips.2023.03.004.

35. Giri, A., Wang, Q., Rahman, I., and Sundar, I.K. (2022). Circadian molecular clock disruption in chronic pulmonary diseases. Trends Mol. Med. *28*, 513–527. https://doi.org/10.1016/j.molmed.2022.04.002.

36. Fu, Y., and Zhuang, X. (2020). m(6)A-binding YTHDF proteins promote stress granule formation. Nat. Chem. Biol. *16*, 955–963. https://doi.org/10.1038/s41589-020-0524-y.

37. Gotor, N.L., Armaos, A., Calloni, G., Torrent Burgas, M., Vabulas, R.M., De Groot, N.S., and Tartaglia, G.G. (2020). RNA-binding and prion domains: the Yin and Yang of phase separation. Nucleic Acids Res. *48*, 9491–9504. https://doi.org/10.1093/nar/gkaa681.

38. Yang, D., Zhao, G., and Zhang, H.M. (2023). m(6)A reader proteins: the executive factors in modulating viral replication and host immune response. Front. Cell. Infect. Microbiol. *13*, 1151069. https://doi.org/10.3389/fcimb.2023.1151069.

39. Frye, M., Harada, B.T., Behm, M., and He, C. (2018). RNA modifications modulate gene expression during development. Science *361*, 1346–1349. https://doi.org/10.1126/science.aau1646.

40. Batista, P.J. (2017). The RNA Modification N(6)-methyladenosine and Its Implications in Human Disease. Dev. Reprod. Biol. *15*, 154–163. https://doi.org/10.1016/j.gpb.2017.03.002.

41. Jiang, X., Liu, B., Nie, Z., Duan, L., Xiong, Q., Jin, Z., Yang, C., and Chen, Y. (2021). The role of m6A modification in the biological functions and diseases. Signal Transduct Target Ther *6*, 74. https://doi.org/10.1038/s41392-020-00450-x.

42. Fang, Q., Tian, G.G., Wang, Q., Liu, M., He, L., Li, S., and Wu, J. (2023). YTHDF1 phase separation triggers the fate transition of spermatogonial stem cells by activating the IkappaB-NF-kappaB-CCND1 axis. Cell Rep. *42*, 112403. https://doi.org/10.1016/j.celrep.2023.112403.

43. Zong, X., Xiao, X., Jie, F., Cheng, Y., Jin, M., Yin, Y., and Wang, Y. (2021). YTHDF1 promotes NLRP3 translation to induce intestinal epithelial cell inflammatory injury during endotoxic shock. Sci. China. Life Sci. *64*, 1988–1991. https://doi.org/10.1007/s11427-020-1909-6.

44. Zhang, S., Guan, X., Liu, W., Zhu, Z., Jin, H., Zhu, Y., Chen, Y., Zhang, M., Xu, C., Tang, X., et al. (2022). YTHDF1 alleviates sepsis by upregulating WWP1 to induce NLRP3 ubiquitination and inhibit caspase-1-dependent pyroptosis. Cell Death Discov. *8*, 244. https://doi.org/10.1038/s41420-022-00872-2.

45. Patke, A., Young, M.W., and Axelrod, S. (2020). Molecular mechanisms and physiological importance of circadian rhythms. Nat. Rev. Mol. Cell Biol. *21*, 67–84. https://doi.org/10.1038/s41580-019-0179-2.

46. Godinho-Silva, C., Domingues, R.G., Rendas, M., Raposo, B., Ribeiro, H., da Silva, J.A., Vieira, A., Costa, R.M., Barbosa-Morais, N.L., Carvalho, T., and Veiga-Fernandes, H. (2019). Light-entrained and brain-tuned circadian circuits regulate ILC3s and gut homeostasis. Nature *574*, 254–258. https://doi.org/10.1038/s41586-019-1579-3.

47. Gray, K.J., and Gibbs, J.E. (2022). Adaptive immunity, chronic inflammation and the clock. Semin. Immunopathol. *44*, 209–224. https://doi.org/10.1007/s00281-022-00919-7.

48. Kou, L., Chi, X., Sun, Y., Han, C., Wan, F., Hu, J., Yin, S., Wu, J., Li, Y., Zhou, Q., et al. (2022). The circadian clock protein Rev-erbalpha provides neuroprotection and attenuates neuroinflammation against Parkinson's disease via the microglial NLRP3 inflammasome. J. Neuroinflammation *19*, 133. https://doi.org/10.1186/s12974-022-02494-y.

49. Wang, S., Lin, Y., Yuan, X., Li, F., Guo, L., and Wu, B. (2018). REV-ERBalpha integrates colon clock with experimental colitis through regulation of NF-kappaB/NLRP3 axis. Nat. Commun. *9*, 4246. https://doi.org/10.1038/s41467-018-06568-5.

50. Wang, Q., Wang, Z., Song, J., Xu, K., Tian, W., Cai, X., Mo, J., Cao, Y., and Xiao, J. (2023). Homogalacturonan enriched pectin based hydrogel enhances 6-gingerol's colitis alleviation effect via NF-kappaB/NLRP3 axis. Int. J. Biol. Macromol. *245*, 125282. https://doi.org/10.1016/j.ijbiomac.2023.125282.

51. Scheiermann, C., Gibbs, J., Ince, L., and Loudon, A. (2018). Clocking in to immunity. Nat. Rev. Immunol. *18*, 423–437. https://doi.org/10.1038/s41577-018-0008-4.

52. Pai, Y.C., Li, Y.H., Turner, J.R., and Yu, L.C. (2023). Transepithelial barrier dysfunction drives microbiota dysbiosis to initiate epithelial clock-driven inflammation. J Crohns Colitis. https://doi.org/10.1093/ecco-jcc/jjad064.

53. Sinclair, C., Bommakanti, G., Gardinassi, L., Loebbermann, J., Johnson, M.J., Hakimpour, P., Hagan, T., Benitez, L., Todor, A., Machiah, D., et al. (2017). mTOR regulates metabolic adaptation of APCs in the lung and controls the outcome of allergic inflammation. Science *357*, 1014–1021. https://doi.org/10.1126/science.aaj2155.

54. Lv, J., Su, W., Yu, Q., Zhang, M., Di, C., Lin, X., Wu, M., and Xia, Z. (2018). Heme oxygenase-1 protects airway epithelium against apoptosis by targeting the proinflammatory NLRP3-RXR axis in asthma. J. Biol. Chem. *293*, 18454–18465. https://doi.org/10.1074/jbc.RA118.004950.

55. Fang, S.B., Zhang, H.Y., Wang, C., He, B.X., Liu, X.Q., Meng, X.C., Peng, Y.Q., Xu, Z.B., Fan, X.L., Wu, Z.J., et al. (2020). Small extracellular vesicles derived from human mesenchymal stromal cells prevent group 2 innate lymphoid cell-dominant allergic airway inflammation through delivery of miR-146a-5p. J. Extracell. Vesicles *9*, 1723260. https://doi.org/10.1080/20013078.2020.1723260.

56. Liu, L., Wang, J., Sun, G., Wu, Q., Ma, J., Zhang, X., Huang, N., Bian, Z., Gu, S., Xu, M., et al. (2019). m(6)A mRNA methylation regulates CTNNB1 to promote the proliferation of hepatoblastoma. Mol. Cancer *18*, 188. https://doi.org/10.1186/s12943-019-1119-7.

57. Liu, J., Eckert, M.A., Harada, B.T., Liu, S.M., Lu, Z., Yu, K., Tienda, S.M., Chryplewicz, A., Zhu, A.C., Yang, Y., et al. (2018). m(6)A mRNA methylation regulates AKT activity to promote the proliferation and tumorigenicity of endometrial cancer. Nat. Cell Biol. *20*, 1074–1083. https://doi.org/10.1038/s41556-018-0174-4.

58. Kang, J.Y., Wen, Z., Pan, D., Zhang, Y., Li, Q., Zhong, A., Yu, X., Wu, Y.C., Chen, Y., Zhang, X., et al. (2022). LLPS of FXR1 drives spermiogenesis by activating translation of stored mRNAs. Science *377*, eabj6647. https://doi.org/10.1126/science.abj6647.

59. Patil, D.P., Chen, C.K., Pickering, B.F., Chow, A., Jackson, C., Guttman, M., and Jaffrey, S.R. (2016). m(6)A RNA methylation promotes XIST-mediated transcriptional repression. Nature *537*, 369–373. https://doi.org/10.1038/nature19342.

60. Xu, C., Liu, K., Ahmed, H., Loppnau, P., Schapira, M., and Min, J. (2015). Structural Basis for the Discriminative Recognition of N6-Methyladenosine RNA by the Human YT521-B Homology Domain Family of Proteins. J. Biol. Chem. *290*, 24902–24913. https://doi.org/10.1074/jbc.M115.680389.

61. Zhang, H., Elbaum-Garfinkle, S., Langdon, E.M., Taylor, N., Occhipinti, P., Bridges, A.A., Brangwynne, C.P., and Gladfelter, A.S. (2015). RNA Controls PolyQ Protein Phase Transitions. Mol. Cell *60*, 220–230. https://doi.org/10.1016/j.molcel.2015.09.017.

STAR★METHODS

KEY RESOURCES TABLE

REAGENT or RESOURCE	SOURCE	IDENTIFIER
Antibodies		
METTL3	Abcam	ab195352 RRID:AB_2721254
METTL14	Abcam	ab220030 RRID:AB_2893210
WTAP	ABclonal	A14695 RRID:AB_2761570
YTHDF1	Abcam	ab252346 RRID:AB_252346
YTHDF1	Servicebio	GB111390
YTHDF2	Abcam	ab246514 RRID:AB_2891213
YTHDF3	Abcam	ab220161 RRID:AB_2868574
CD326	Abcam	ab71916 RRID:AB_1603782
CLOCK	ABclonal	A7265 RRID:AB_2863594
CRY2	ABclonal	A17465 RRID:AB_2769052
PER2	ABclonal	A5107 RRID:AB_2863447
PER3	ABclonal	A2219 RRID:AB_2862977
CREB1	ABclonal	A11064 RRID:AB 2758389
FBXL3	Abcam	Ab96645 RRID:AB 10679381
TSLP	Servicebio	GB111664
IL-25	Abcam	Ab115672 RRID:AB 10902345
IL-33	Affinity	DF8369 RRID:AB 2841633
NLRP3	Cell Signaling Technology	1510S
NLRP3	Servicebio	GB11300
IL-1β	Abcam	Ab234437 RRID:AB 2936228
Biological samples		
Human bronchial biopsies samples	This study	N/A
Chemicals, peptides, and recombinant proteins		
TRIZOL reagent	Thermo Fisher scientific	15596018
LipoFectamine 3000	Thermo Fisher scientific	L3000150
HaltTM protease and phosphatase inhibitor cocktail	Thermo Fisher scientific MedChemExpress	78440 HY-K0021
Triton X-100	Beyotime	P0096
RIPA	Beyotime	P0013B
Magna RIP™ RNA-Binding	Millipore	17–701
House Dust Mite	Greer labs	XPB82D3A25
PneumaCult™ -Ex Plus Medium	STEMCELL Technologies	05040
PneumaCult™-ALI Medium	STEMCELL Technologies	05001
Pronase	MedChemExpress	HY-114158
penicillin/streptomycin	Thermo Fisher Scientific	15140122
fungizone	Thermo Fisher Scientific	15290026
Collagen I, Rat Tail	Merck-Millipore	18080093
SYBR® Green PCR Master Mix	Thermo Fisher Scientific	23225
DAPI	Sigma-Aldrich	D9542
Critical commercial assays		
FastQuant RT Kit	TIANGEN	KR106
Pierce™ BCA Protein Assay Kit	Thermo Fisher Scientific	F6057

(*Continued on next page*)

Continued		
REAGENT or RESOURCE	SOURCE	IDENTIFIER
Deposited data		
m6A-Seq, mRNA-Seq	This study	GSE256458, GSE256531
Experimental models: Cell lines		
Primary human AECs	This study	N/A
Primary mouse AECs	This study	N/A
BEAS-2B	This study	N/A
Experimental models: Organisms/strains		
Mouse: C57/BL6	The Jackson Laboratory	RRID:IMSR JAX:000664
Mouse: BALB/c	The Jackson Laboratory	RRID:MGI:2161072
Mouse: YTHDF1$^{fl/fl}$		N/A
Mouse: Shh^{cre}		N/A
Oligonucleotides		
Primers are listed in Table S2	This study	N/A
siRNA sequence are listed in Table S3	This study	N/A
Recombinant DNA		
YTHDF1-Flag	This study	N/A
YTHDF1-YTH-mut	This study	N/A
YTHDF1-C	This study	N/A
BFP-YTHDF1-C	This study	N/A
Software and algorithms		
Imaris	Bitplane	https://imaris.oxinst.com/packages
Prism	GraphPad	https://www.graphpad.com/scientific-software/prism
FlowJo	FlowJo	https://www.flowjo.com
ImageJ	ImageJ	https://imagej.net/ij/

RESOURCE AVAILABILITY

Lead contact

Further information and requests for resources and reagents should be directed to the lead contact, Zhenwei Xia (xzw10484@rjh.com.cn).

Materials availability

This study did not generate new unique reagents.

Data and code availability

- All original data will be available upon contacting lead contact.
- The m6A-Seq and mRNA-Seq data associated with this study have been deposited at GEO and are publicly available as of the date of publication. Accession number is listed in the key resources table.
- Any additional information required to reanalyze the data reported in this paper is available from the lead contact upon request.

EXPERIMENTAL MODEL AND STUDY PARTICIPANT DETAILS

Experiments were performed on female mice between 6 and 8 weeks of age unless other specified, Wild type C57/BL6 mice and BALB/c mice were purchased from the Jackson Labs. To generate *YTHDF1$^{fl/fl}$shh$^{cre/+}$* mice, *YTHDF1$^{fl/f}$ mice and shh^{cre}* mice were purchased from Shanghai Model Organisms Company. All animal experiments were carried out in accordance with the National Institutes of Health Guide for the Care and Use of Laboratory Animals, with the approval of Ruijin Hospital, Shanghai Jiao-tong University School of Medicine (Shanghai, China).

Human bronchial biopsies samples were obtained from 23 asthmatic patients and 18 control subjects. The asthmatic donors all had a formal diagnosis of asthma made by a medical practitioner according to the Global Initiative for Asthma guidelines (GINA). The control subjects recruited for this study with normal lung function, defined as forced expiratory volume in 1 s (FEV_1)/forced vital capacity (FVC)>lower limit of normal (LLN), FEV_1>80% predicted. The control subjects had no history of asthma or allergy. The research

was approved by the Ethics Committee of Ruijin Hospital, Shanghai Jiao Tong University School of Medicine (Shanghai, China) (No. 2019-YK061). All participants signed an informed consent form prior to the study. The clinical information is shown in Table S1.

METHOD DETAILS

pAECs isolation from mice

pAECs were isolated from mice bronchial main branches digested in 1.5 mg/mL pronase (MedChemExpress). Briefly, tracheas were harvested from mice and placed into 30 mL of Ham's F12 medium (Thermo Fisher Scientific) containing 1% penicillin/streptomycin (Thermo Fisher Scientific) and 1% fungizone (Thermo Fisher Scientific) and cut along the vertical axis to expose the lumen and transferred to a new 50 mL tube containing 10 mL Ham's F12 medium with 1% antibiotic and 1.5 mg/mL pronase, then incubated on a roller at 4°C overnight. Next day, 10 mL of Ham's F12 medium containing 20% FBS and antibiotics were added and inverted the tube 10 times. Then, 70 μm strainer were used to filter the cells in the tube. All solutions were combined and centrifuged at 1,400 rpm for 10 min at 4°C. The cell pellets were resuspended in Ham's F12 medium containing 1% antibiotics. Cells were then plated into culture dish before incubation at 37°C, 5% CO_2 for 5 h to negatively select fibroblasts. The supernatant was collected and centrifuged at 1,400 rpm for 10 min at 4°C. Cell pellets were then cultured in a six-well tissue culture plate (Corning) and coated with Collagen I, Rat Tail (MERCK) at 37°C, 5% CO_2 for 7 days.

Allergic stimulation of pAECs

For models of pAECs stimulated by allergens in humans and mice, we first extracted primary airway epithelial cells from control human subjects and naive mice, respectively, and then stimulate pAECs with 40 μg/mL HDM or 1 mg/mL OVA for 24 h.

ALI (air-liquid interface) culture of pAECs

Tissues were incubated in medium containing 1.4 mg/mL protease and 0.1 mg/mL DNase for 1 h at 37°C. The proteases were neutralized with medium containing 10% FBS and resulting suspension of cells was incubated in a flask at 37°C, 5% CO_2 for 2 h in PneumaCult-Ex Plus medium (STEMCELL) with 100 U/ml penicillin and 100 μg/mL streptomycin to remove non-epithelial cells. After 2 h, cells were propagated in PneumaCult-Ex Plus medium. For differentiation, cells were grown in air-liquid interface (ALI) cultures exposure in PneumaCult-ALI medium (STEMCELL).

ELISA

To obtain lung homogenate, whole lungs were dissociated in 1 mL PBS containing 0.05% Triton X-100, protease and phosphatase inhibitor cocktail(MedChemExpress). Suspensions were passed through a 40 mM cell strainer and clarified by 3,000 rpm centrifugation. Supernatant was used for detecting cytokines by ELISA.[53] To obtain serum, blood was obtained by eye ball blood collection, centrifuged blood for 1,000 rpm. The levels of IgE, IL-4, IL-5 and IL-13 were measured with ELISA kit (Abcam or Biolegend) according to the manufacturer's instructions. The OD at 450 nm and 595 nm was recorded.

RNA isolation and RT-qPCR

Total RNA was isolated with TRIzol reagent (Thermo Fisher scientific) following the manufacture's instructions. Total RNA was reverse transcribed into cDNA using SuperScript®III Reverse Transcriptase (Thermo Fisher scientific). Quantitative RT-qPCR was performed using SYBR® Green PCR Master Mix with the StepOne Real-Time PCR System (Applied Biosystem). GAPDH and 18s were used as an internal control for the normalization. Relative changes in expression were calculated using the ΔΔCt method. Primers of interested gene used in this research are listed in Table S2.

Transfection and siRNA knockdown

Transfection of plasmids was performed using Lipofectamine 3000 (Thermo Fisher scientific) according to the manufacturer's instructions. Transient knockdown of target genes by siRNA was performed with LipoFectamine RNAi Max (Thermo Fisher scientific. siRNA oligonucleotides specific for siYTHDF1 and siCLOCK were designed and synthesized from Genomeditech. The siRNA sequences were listed in Table S3.

Protein extraction and western blotting

Whole cells were homogenized in RIPA buffer (Beyotime) supplemented with 1% protease inhibitor cocktail (Thermo Fisher Scientific) and phosphates inhibitor cocktail (Thermo Fisher Scientific). After centrifuged at 12,000 rpm for 10 min at 4°C, the supernatant of lysates was collected and determined by Pierce BCA Protein Assay Kit (Thermo Fisher scientific).[54,55] The protein was run on an SDS-PAGE gel and transferred to a nitrocellulose membrane. Nitrocellulose membranes were blocked in 5% BSA and probed with the following antibodies overnight: METTL3 (Abcam); METTL14 (Abcam); WTAP (Abcam); YTHDF1 (Abcam); YTHDF2 (Abcam); YTHDF3 (Abcam); GAPDH (Proteintech); CLOCK (ABclonal) were followed by enhanced chemiluminescence (Thermo Fisher scientific). Results were confirmed by at least three independent experiments.

Immunohistochemistry

Harvested tissues were fixed in 4% formaldehyde, embedded in paraffin, and sliced longitudinally into 4 μm thick sections. Immunoreactivity in sections were stained with indicated primary antibodies and secondary antibodies. The areas of positive immunolabeled regions were quantified by using ImageJ image analysis software.

Immunofluorescence imaging

The collected lung tissue was embedded in paraffin and sliced at a thickness of 5 μm. After dewaxing, the samples were then permeabilized with 0.1% Triton X-100 (prepared in PBS) at room temperature for 15 min. To block non-specific binding, samples were blocked with PBS containing 10% normal goat serum for 1 h at room temperature, and then was incubated overnight at 4°C with the primary antibody. After three washes with PBS, the corresponding fluorescence-labelled secondary antibodies were applied to stain the cells and incubated for 1 h. The nuclei were counterstained by mounting the cells in 4,6-diamidino-2-phenylindole (DAPI; Sigma-Aldrich). The immunofluorescence signals were photographed using a confocal laser scanning microscope (Carl Zeiss LSM 880).

LC-MS/MS quantification of m6A in poly(A)-mRNA

The total RNA from indicated cells was isolated using TRIzol reagent (Thermo Fisher Scientific) following to the manufacturer's instructions. mRNAs (100–200 ng) were digested by 4 μL nuclease P1 (Sigma-Aldrich) in 25 μL buffer solution containing 10 mM Tris-HCl pH 7.0, 25 mM NaCl, 2.5 mM ZnCl2 at 37°C for 12 h, followed by incubating with 1 μL alkaline phosphatase (Sigma-Aldrich) at 37°C for 2 h. The sample was then filtered (0.22 μm pore size, 4 mm diameter, Millipore), and 5 μL solution was injected into LC-MS/MS. The nucleosides were separated by reverse phase high-performance liquid chromatography on an Agilent C18 column, coupled with mass spectrometry detection using AB SCIEX QTRAP 5500. The m6A levels were calculated as the ratio of m6A to A based on the calibrated concentrations according to the standard curve obtained from pure nucleoside standards running with the same batch of samples.

m6A-seq and mRNA sequencing

Mouse AECs were isolated by fluorescence-activated cell sorting (FACS) using CD326-FITC (Thermo Fisher scientific), CD45-APC (BD Biosciences). Total mRNA was extracted from mouse AECs. Then, mRNA sequencing and m6A sequencing were simultaneously performed (Cloud-Seq Biotech, Shanghai, China). For mRNA sequencing, mRNAs were single-end sequenced on Ilunina HiSeq 2000 machines. Transcript assembly and differential expression were examined by unsing Cufflinks with Refseq mRNA to guide assembly. For m6A sequencing, mRNA was randomly fragmented to ~200 nucleotides by RNA fragmentation reagents. 500 μg of fragmented mRNAs were saved as input control for RNA-Seq, 500 μg of fragmented mRNAs were incubated with 5 μg of anti-m6A polyclonal antibody (Synaptic System, diluted to 0.5 μg/μL) in IPP buffer (150 mM NaCl, 0.1% NP-40, 10 mM Tris–HCl, pH 7.4) for 2 h at 4°C. The mixture was then incubated with beads and eluted with elution buffer (1×IP buffer and 6.7 mM m6A). Eluted mRNA was precipitated by 75% ethanol and treated with RNasin (Ambion) according to the manufacturer's instructions. TruSeq Stranded mRNA Sample Pre Kit (Illumina) was used to construct the library from immunoprecipitated mRNA and input mRNA following to a published protocol. Both the input sample (without immunoprecipitation) and the m6A IP sample were subjected to 150 bp paired-end sequencing on Illumina HiSeq sequencer HiSeq sequencer.[56,57]

RNA immunoprecipitation (RIP)

Cells were collected and washed twice with cold PBS, then lysed in ice-cold IP lysis buffer (50 mM Tris-HCL pH 7.5; 300 mM NaCl and 0.5% NP40) for 30 min on ice and frozen down at −80°C immediately to aid the lysis. For the immunoprecipitation, lysate was thawed out and spin down at max speed to precipitate the debris at 4°C. Supernatant was collected and incubated with 8 μg anti-FLAG antibody (Abcam) or equivalent amount of Rabbit IgG (Millipore) by rotating overnight at 4°C. Protein A/G magnetic beads (Millipore) were used to pull down RNA-YTHDF1-antibody. Followed by three washes with RIP buffer. RNA was extracted using TRIzol reagent (Thermo Fisher scientific) following the manuscript's instructions.

Polysome profiling

Cells were incubated with 100 g/mL cycloheximide (CHX, Merck Millipore) at 37°C for 15 min, pelleted and lysed on ice in lysis buffer (20 mM HEPES pH 7.6, 100 mM KCl, 5 mM $MgCl_2$, 1% Triton X-100, 100 μg/mL cycloheximide), supplemented with protease inhibitor and RNase inhibitor then centrifuged. The supernatant was collected, loaded onto a 10/50% (w/v) sucrose gradient solution prepared in lysis buffer, then centrifuged at 4°C for 4 h at 27,500 rpm. The sample was fractioned and analyzed using a Gradient Station (BioCamp) equipped with an ECONO UV monitor (BioRad) and fraction collector (Gilson). RNA was purified by Trizol from each fraction and subjected to RT-qPCR analysis.

FRAP assay

FRAP experiments were performed on a white light laser confocal microscopes equipped with immersion objectives of 63×magnification driven by the imaging software provided by the manufactures. For FRAP experiments in living cells, cells were plated on a 35-mm dish with a glass-like polymer bottom (Cellvis). The images were taken and the regions of interest were photobleached. Each

data point is representative of the mean and standard deviation of fluorescence intensities in three unbleached or three bleached granules.[29,58]

Protein expression and purification

N-terminal 6X-His tagged YTHDF1 was generated by standard PCR-based cloning strategy from HEK293T oligo-d(T)25-primed cDNA.[59] Recombinant YTHDF1 proteins were expressed in E. coli Rosetta2 (DE3) single (Novagen) using pET-28(+) (Novagen) or pProEx HTb (Thermo Fisher scientific). E. coli expressing YTHDF1 proteins were induced with 0.5 mM isopropyl β-D-1-thiogalacto-pyranoside (IPTG) at 18°C overnight, harvested by centrifugation at 4°C, then lysed in the following buffer: 50 mM NaH_2PO_4 pH 7.2, 300 mM NaCl, 20 mM imidazole at pH 7.2 and supplemented with EDTA-free protease inhibitor cocktail (Roche). Bacterial lysate was clarified by centrifugation at 15,000 rpm for 40 min. The supernatant of recombinant YTHDF1 protein was purified using Talon Metal Affinity Resin (Clontech) and eluted in the following buffer: 50 mM NaH2PO4 pH 7.2, 300 mM NaCl, 250 mM imidazole-HCl at pH 7.2. Further concentration and buffer exchange was performed using Amicon Ultra-4 spin columns (Merck-Millipore). Recombinant protein was stored in the following buffer: 20 mM HEPES pH7.4, 300 mM KCl, 6 mM $MgCl_2$, 0.02% NP40, 50% glycerol at −80°C or 20% glycerol at −20°C. The purified protein was quantified using an ND-2000C NanoDrop spectrophotometer (NanoDrop Technologies) with OD 280 and verified by Coomassie staining.

Protein labeling

Alexa Fluor 488 Microscale Protein Labeling kit (Thermo Fischer Scientific) was used to fluorescently label YTHDF1. According to the manufacturer's instruction, YTHDF1 proteins were diluted at 1 mg/mL in PBS a mixed with 100 mM sodium bicarbonate. Purified fluorescently labeled proteins from the unreacted dye substrate by column purification using Micro Bio-Spin Columns with P-30 gel. The labeled YTHDF1 proteins were eluted in the buffer containing 20 mM HEPES pH 7.4, 300 mM KCl, 6 mM $MgCl_2$, 0.02% NP-40.

Droplet formation

The Alexa Fluor 488 labeled YTHDF1 proteins were eluted in a buffer with a gradient of NaCl buffer (20 mM HEPES pH 7.4, 300 mM KCl, 6 mM $MgCl_2$, 0.02% NP-40, 50% glycerol, with NaCl) on a coverslip by observation using microscope.[60,61]

TRICK reporter assay

The CLOCK TRICK reporter was constructed by engineered PP7 binding sites (PBS) or MS2 binding sites (MBS), the binding motifs for PP7 coat protein (PCP) and MS2 coat protein (MCP), into the coding and 3′ untranslated region of CLOCK, respectively. Because translating ribosomes can displace RBP binding to the coding region, PCP targeted to the coding region through the inserted PBS motif thus can act as a biosensor to distinguish translated mRNAs from untranslated ones. For the CLOCK TRICK reporter assay, CLOCK TRICK reporter was cotransfected with the expression vectors for GFP-NLS-PCP, RFP-NLS-MCP, and BFP-YTHDF1 or its mutant in BEAS-2B cells.

QUANTIFICATION AND STATISTICAL ANALYSIS

Statistical analysis was performed using Graph-Pad statistical software version 9 (GraphPad Software Inc.). Error bars show mean ± SEM. Student's t tests were used for comparison between two groups. For experiments with more than two conditions, one-way or two-way Analysis of variance (ANOVA) was used for comparisons between all groups. Pearson's correlation analyses were used to analyze correlations. Receiver operator characteristics (ROC) curves were constructed to examine the relationship between sensitivity and specificity. And the area under the curve (AUC) was calculated to assess the overall performance of YTHDF1. The ROC curves were performed by Meta-Disc version 1.4. $p < 0.05$ was considered significant (*$p < 0.05$, **$p < 0.01$, ***$p < 0.001$, ****$p < 0.0001$, n.s., not statistically significant).